SPAR WIND TURBINE BEHAVIOR: MODELING AND COMPARISON WITH EXPERIMENTAL DATA

A Thesis

by

HE YANG

Submitted to the Office of Graduate and Professional Studies of
Texas A&M University
in partial fulfillment of the requirements for the degree of

MASTER OF SCIENCE

Chair of Committee,	John M. Niedzwecki
Committee Members,	Jun Zhang
	H. Joseph Newton
Head of Department,	Robin Autenrieth

December 2015

Major Subject: Ocean Engineering

ABSTRACT

The potential for the development of offshore wind farms for deep water has inspired new designs of floaters that could survive harsher environments. Among all of the proposed designs, spar-type wind turbine appears to be a viable concept. The research work presented in this thesis utilizes two types of hydrodynamic numerical models to simulate the global motion response behavior.

The first model developed in this study provides global response information of a spar-type floater in both frequency and time domains. It located the body-coordinate at the net mass center, including structural mass and hydrodynamic added mass. The platform behavior was evaluated from both linear and non-linear forms of Morison's Equation. The second model utilized industry standard software for response analysis. It coupled OrcaFlex software with mean-drift and full QTFs computed by WAMIT software. It provided fully nonlinear hydrodynamic simulation of the spar-type wind turbine and allowed the assessment of the wind effect on the whole floating system.

A model test was recently conducted in the State Key Lab of Ocean Engineering at Shanghai Jiao Tong University. It involved the study of NREL (National Renewable Energy Lab) 5MW baseline wind turbine atop the OC3-Hywind spar-buoy, working in a water depth of 200m. The global motions predicted using the numerical models were compared with the experimental measurements. The first model worked well for the wave-frequency range while the second model worked well for the whole frequency range which is needed for floating wind turbine simulations. It was observed that effect of the wind influenced the damping of the long period drifting motion, while the forced motion in wave-frequency range was not significantly influenced.

ACKNOWLEDGEMENTS

I would like to show my gratitude to my chair of advisory committee, Dr. John M. Niedzwecki, who helps me to develop the critical thinking and self-discipline as an independent researcher, trains me from a freshmen into a young engineer in ocean engineering, and encourages me to explore more possibilities for my academic life. I thank him for teaching me the necessary research methods and inspiring my own fresh thoughts at the same time. I would also like to extend my thankfulness to my committee members, Dr. Jun Zhang and Dr. H. Joseph Newton, for their great support and guidance throughout my master studies.

I gratefully acknowledge the technical support from State Key Lab of Ocean Engineering in Shanghai Jiao Tong University. Dr. Jianmin Yang, Dr. Runpei Li, and Dr. Zhiqiang Hu have provided precious experimental documents and very insightful discussion.

Thanks also go to my classmates in 2013 ocean engineering program, the nice and helpful faculty in the Civil Engineering Department, and all of my friends who give me endless encouragement during the past two years. Finally, I would like to thank my dear parents, who give me the warmest support in my life. It is their love and caring that guide me to pursue my dream in this foreign country. Thank you so much!

TABLE OF CONTENTS

LIST OF FIGURES

LIST OF TABLES

1. INTRODUCTION

During the past several decades, global offshore oil and gas resources have been sought to meet the sharply increasing demand of these traditional energy sources. At the same time, the huge emission of greenhouse gas has renewed worldwide in developing environmental friendly renewable energy. Wind, which is clean and renewable, shows a great of advantages. For underdeveloped areas, such as mountainous regions and remote islands where electricity grid is unreachable, wind energy could prove to be an effective solution. Developing countries are also increasing their fossil fuel consumption and wind energy could be more easily integrated into their future energy structure. Intensively, the cost of wind power generation significantly decreased to one fifth of that in the 1960s, and thus the economics of wind energy are improving.

1.1 Offshore Wind Turbine Background

The onshore wind energy industry has blossomed around the world with the wind farm technology dominated by Europe. However, the locations of wind turbine onshore or in coastal region use limited land resources and this has led to undesirable visual and acoustic impact, which encourages the desire to place the wind farms far offshore at deep water sites. Compared with onshore wind energy resource, offshore wind resource is steadier. Moreover, different from European countries, whose wind energy development are concentrated on the shallower coastal areas, North America has high-quality wind in offshore areas deeper than 30 to 50 meters, where wind turbine will be subject to harsher environmental conditions. Thus, development of offshore wind energy technique in intermediate and deeper water sites turns out to be of great significance. Breton and Moe (2009) review the challenges and technologies for offshore wind turbines in Europe and North American comprehensively.

Although both onshore wind farms and floaters for oil and gas industry have been operating successfully in harsh environments, offshore wind turbine is by no means the

simple assembly of these two parts. The harsh environment of ocean means that various working loads as well as installation and maintenance will be challenging. Thus large wind turbine design has been proposed to make up for this higher costs, and may also bring about unwanted aerodynamic impact on the floater. Larger wind turbines will resort in the larger floater size and deeper draft to provide enough stability for the whole system. Considering such specific design conditions for offshore wind turbine, optimal design should balance all these factors to maximize the overall performance of whole system, rather than directly copying from existing design principles for traditional onshore wind turbine and platforms.

Wang et al. (2010) and Butterfield et al. (2005) have published excellent review papers about different wind turbine floater concepts. Traditionally, monopiles or gravity based foundation are among the best choices for wind turbines in shallow water areas. Whereas, wind turbine floaters for deep water are categorized according to their balance of stability options, which include a spar-type buoy called Hywind developed by Statoil of Norway, a barge designed by Massachusetts Institute of Technology (MIT), a TLP created by the University of Maine, and a semi-submersible platform. However, each of them has merits and demerits with respect to their hydrodynamic performances. Actually current designs for offshore wind turbine floaters are always the combination of several concepts in order to achieve an optimal static performance.

Among all types of offshore wind turbine floaters, spar-type floaters have several advantages. First, its large ballast associated with its large draft, which is at least equal to the height of tower, greatly lowers its center of gravity and thus provides a huge righting moment arm. This explains its high inertia resistance to pitch and roll motions. Second, combined with a taut or a catenary spread mooring system, yaw motions are highly damped, making such moored spar-type wind turbine design a very suitable option for water depth larger than 200 meters. Third, compared with other complicated hull shape designs, spar-based systems are relatively easy to manufacture and convenient to transport to the wind farm site. This also shows that spar-buoy is a financially competitive concept.

1.2 Offshore Code Comparison Collaboration Project (OC3)

To better estimate the properties of offshore wind turbines that are coupled with different floaters, the National Renewable Energy Laboratory (NREL) in the U.S. proposed an Offshore Code Comparison Collaboration Project (OC3). Jonkman et al. (2010) briefly introduced the planning of this project in the summary report from NREL. OC3 project provides the opportunity to discuss wind turbine modeling strategies, benchmark numerical models and compare the numerical predictions based on different numerical approaches. Participants from more than ten universities and research institutions are joining in this project. It is divided into 4 phases that address wind turbine response modeling on monopole structures with rigid foundations (Phase I), monopole structures on flexible foundations (Phase II), tripod structures (Phase III), and floating platforms (Phase IV). Figure 1.1 below shows the development of the OC3 project.

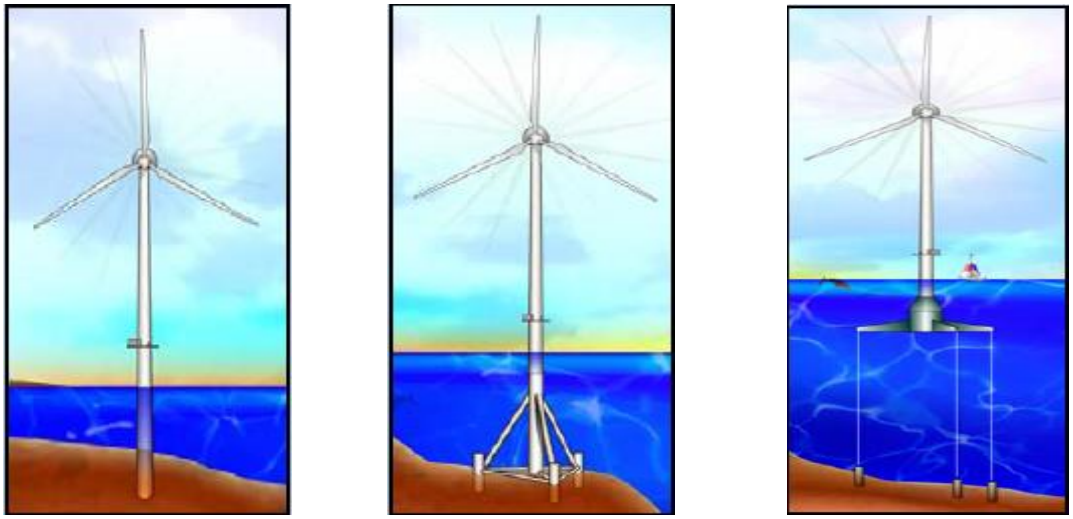

Fig 1.1 Offshore Code Comparison Collaboration Project (OC3) development (Butterfield et al, 2005)

For each phase, in order to make results from different institutions comparable and better figure out the origin of differences between code predictions, all the inputs for the wind turbines, predefined floaters and working conditions are controlled. The OC3 project uses the publicly available 5MW baseline wind turbine released by NREL. The aerodynamic rotor properties, together with nacelle, blade, drivetrain, and the tower elastic properties, are all given in details. In addition, floaters and mooring systems applied to support the wind turbine in each phase is also identical for all the participants. It should be noted that, current phase of OC3 project hasn't taken cost evaluation into consideration, so that more conservative designs, like deep draft spar-type floater Hywind, are adopted. Various combination of wind, wave and current loads are selected as uniform simulation input.

Each of the participants' coupled simulation models address the coupled response behavior due to the aerodynamics, hydrodynamics, structural dynamics and control systems associated with offshore wind turbine systems. Table 1.1 is developed by NREL, which identifies the participants and provides an overview of the methodologies the participants utilized in the OC3 project. As shown in the table, the aerodynamic modules were mainly based on blade element theory (BEM), while hydrodynamic modules incorporated airy wave theory, several used potential flow theory, and all used the Morison's equation.

Table 1.1 Comparison of Numerical Simulation Tools for OC3 Participants (Jonkman et al, 2010)

FAST	Bladed	ADAMS	HAWC2	3Dfloat	Simo	SESAM/DeepC
Code Developer						
NREL	GH	MSC + NREL + LUH	Risø-DTU	IFE-UMB	MARINTEK	DNV
OC3 Participant						
NREL + POSTECH	GH	NREL + LUH	Risø-DTU	IFE-UMB	MARINTEK	Acciona + NTNU
Aerodynamics						
(BEM or GDW) + DS	(BEM or GDW) + DS	(BEM or GDW) + DS	(BEM or GDW) + DS	(BEM or GDW)	BEM	None
Hydrodynamics						
Airy+ + ME, Airy + PF + ME	(Airy+ or Stream) + ME	Airy+ + ME, Airy + PF + ME	Airy + ME	Airy + ME	Airy + PF + ME	Airy+ + ME, Airy + PF + ME
Control System (Servo)						
DLL, UD, SM	DLL	DLL, UD	DLL, UD, SM	UD	DLL	None
Structural Dynamics (Elastic)						
Turbine: FEMP + (Modal / MBS), Moorings: QSCE	Turbine: FEMP + (Modal / MBS), Moorings: UDFD	Turbine: MBS, Moorings: QSCE, UDFD	Turbine: MBS / FEM, Moorings: UDFD	Turbine: FEM, Moorings: FEM, UDFD	Turbine: MBS, Moorings: QSCE, MBS	Turbine: MBS, Moorings: QSCE, FEM

Airy^{+} – Airy wave theory; (+) with free surface connections
BEM – blade-element/momentum
DLL – external dynamic link library
DNV – Det Norsk Veritas
DS – dynamic stall

GDW – generalized dynamic wake
FEM^{P} – finite-element method; (P) for mode preprocessing only
MBS – mulibody-dynamics formulation
ME – Morison's Software Corporation

PF – linear potential flow with radiation and diffraction
QSCE – quasi-static catenary equations
SM – interface to Simulink® with MATLAB®
UD – implementation through user-defined subroutine available
UDFD – implementation through user-defined force-displacement relationships

For efficiently calculating hydrodynamic resposne, the frequency-domain analysis was initially applied to floating wind turbine based on traditional oil and gas platform analysis. Using linear assumptions, frequency–domain method characterized response amplitude operator (RAO) for the specific system configuration. In the studies by Bulder (2002) and Lee (2005), floating wind turbine introduced the extra mass, inertia and damping associated with a wind turbine attached to a spreading moored spar hull. By using frequency-domain analysis method, a good design was shown to be one in which natural frequencies of six degree of freedom motions were located outside of the peak frequency range of wave spectrum. However, since the aerodynamic loading on wind turbine as well as the drifting motion of floater is always nonlinear, frequency-domain analysis is not ideal to capture such important properties.

To better capture the nonlinear properties of floating wind turbine, various time-domain simulation tools that include aero-hydro coupling are developed and released by several OC3 participants. Information is exchanged between several numerical simulators for each time step, so that response could be given as a time series corresponding to the specific wind and wave loading conditions. Thus, wind damping effects are accounted for the relative motion at each time step. In addition, for time-domain simulation, the Morison equation drag force is evaluated by the relative velocity between fluid and floater. However, for most of existing time-domain analysis, to save the simulation time of hydrodynamic module, frequency-domain results are saved in advance and mooring system is regarded as a spring system with static stiffness. Thus, for each time step, given the six DOF motion, hydrodynamic forces are given by extrapolation of these saved parameters.

For the offshore 5MW Baseline OC3 Hywind wind turbine released by NREL in 2007, all of the OC3 project participants ran coupled simulations with their own tools. NREL collected all of their simulation results and compared with each other to testify the consistency. In the U.S., Jonkman et al. (2007) extended FAST (Fatigue, Aerodynamics, Structures, and Turbulence), a code originally written for onshore wind turbine, into a fully coupled package for offshore wind turbine. They calculated aerodynamic and hydrodynamic loading separately in AeroDyn and HydroDyn and input them simultaneously into the structural dynamic calculator ADAMs with fine divided body grids. Motions amplified by extra loading of wind and damping, like pitch and yaw, were characterized and compared with traditional onshore turbine, in order to suggest design modifications and control methodologies.

Their counterpart in Norway, Kirimirad and Moan (2011, 2012), published a series of papers related to this 120m draft spar-buoy mounted by 5-MW wind turbine. They simulated the wave- and wind-induced motion of response in operational and extreme survival conditions. It was found that wind force determines the resonance of the large motion, which is the key to structure’s maximum lifetime. In their following

studies, they also use another tension leg spar-type wind turbine to make code-to-code comparison between HAWC2 and USFOS/vpOne.

In order to validate these coupled simulation tools and further explore dynamic behaviors not shown in the numerical results, several wave basin tests were conducted in Maritime Research Institute Netherlands (MARIN), the Norwegian Technology Research Institute (MARINTEK), and State Key Lab of Ocean Engineering (SKLOE) at Shanghai Jiao Tong University independently. A large number of tests were performed ranging from free-decay tests to complex operating conditions with irregular sea states and dynamic winds. Recorded data include rotor torque and thrust, tower top and base forces and moments, 6 DOF platform motions, and mooring line tensions.

Koo and et.al (2012, 2012) published part of the experimental data measured in the model tests for three different floaters in MARIN. Besides the system identification test results which testify designed properties for the system, they mainly presented the motion response amplitude operator (RAO) with and without wind in order to figure out wind effect on the whole floating wind turbine system. Figure 1.2 shows their experimental results with and without wind loading. NREL (2013) also published their predictions in FAST to reveal the predicted wind effect on the three floating wind turbine systems. Figure 1.3 shows RAOs of surge and pitch motions derived from FAST coupled simulation under white noise wave with and without wind. For experimental results collected in MARINTEK, Skaare et al (2007) compared it with their simulation results from SIMO/RIFLEX/HAWC2 integrated tool. It should be also mentioned that in Japan, Utsunomiya et al (2009, 2009, 2013) designed their own spar-type wind turbine and conducted a series of model tests with different scale ratio. They published several papers which estimated their spar-type wind turbine behavior based on the Morison's equation only.

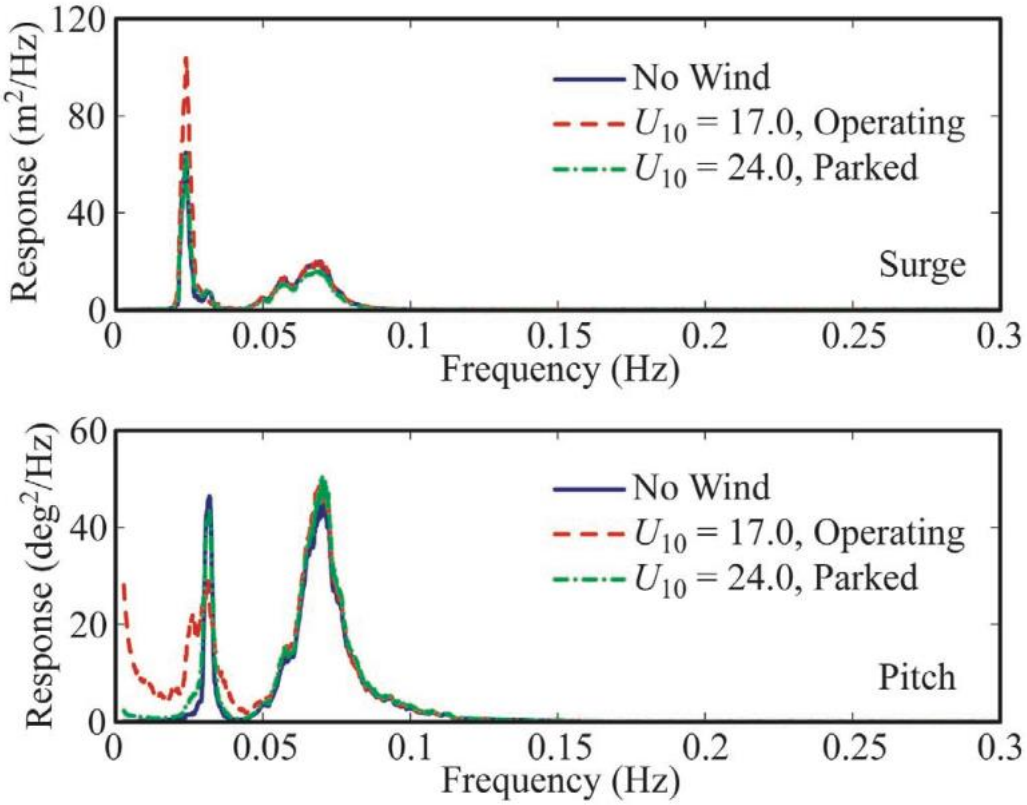

Fig 1.2 Spar-buoy surge and pitch response spectra for an Hs=10.5m sea state with three conditions (Koo et al, 2012)

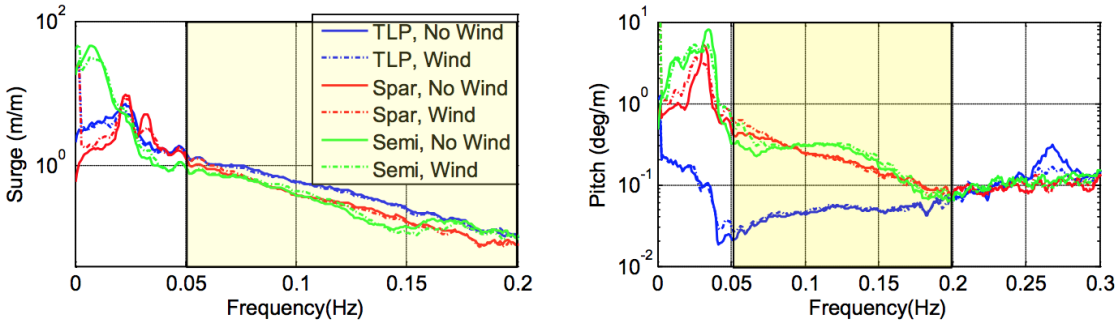

Fig 1.3 RAOs derived from FAST under white noise wave with 7.1m wave height with/without wind (Robertson et al, 2013)

Moreover, NREL (2013) also published the comparisons between their coupled simulation results from FAST and MARIN wave basin tests. Figure 1.4 below shows the RAOs of surge and pitch motion while figure 1.5 shows the comparison curves for predicted and measured mooring line tensions.

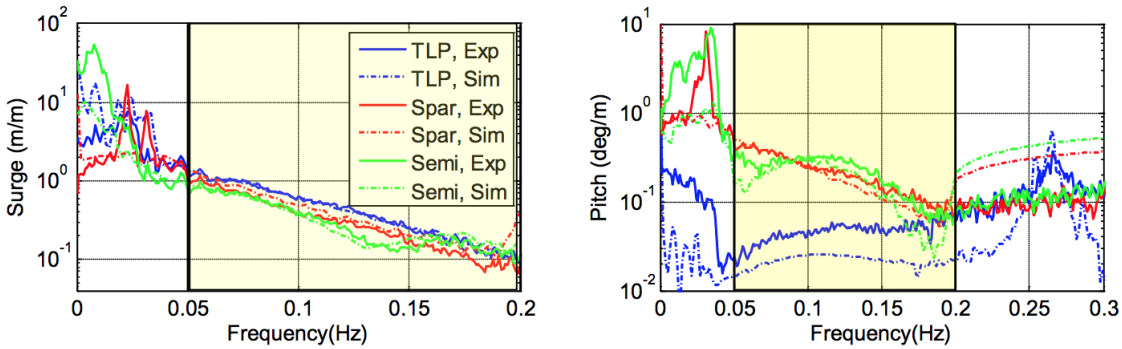

Fig 1.4 RAOs derived from white noise wave with 7.1m wave height without wind by FAST & experiment (Robertson et al, 2013)

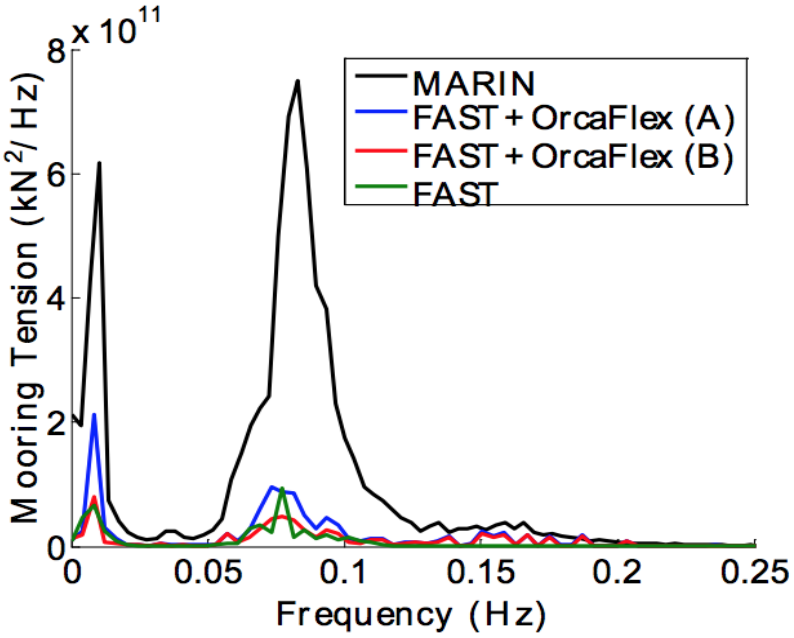

Fig 1.5 Mooring line forces for a wave-only case, Hs=7.04m, Tp=12.18s, JONSWAP spectrum (Robertson et al, 2013)

In the surge and pitch response spectra provided by MARIN wave basin tests, it is shown that for cases with parked wind turbine, the response is almost identical with cases without wind. Meanwhile, for cases that wind turbine operates under a certain steady wind, peaks in wave frequency range remain the same with cases without wind loading, while peaks in low frequency range show a significant change. However, the simulation results from FAST doesn't reveal such an important change induced by steady wind. In figure 2, curves of RAOs with and without wind fit closely in both wave frequency and low frequency ranges.

Thus, the comparisons of these time-domain numerical tools with the corresponding wave basin tests prove their feasibility only under a certain specific assumptions. And even though numerical and experimental results match well in wave-frequency range, low-frequency range shows a great discrepancy, since, as mentioned above, most of the existing state-of-the-art tools for aero-hydro-servo-elastic dynamics simulation for floating wind turbine consider only the first-order wave-excitation loads. However, the significant slow-drifting motion of spar-type buoy is known to be induced by second-order wave-excitation forces. On one hand, the difference-frequency wave loads excite slow drift motions in slack moored system; on the other hand, for floating wind turbine, sum-frequency loads may excite the first tower-bending modes. Thus, to fully understand the response of floating wind turbine as well as the wind damping effect in low-frequency range, a higher order hydrodynamic analysis is of great importance.

1.3 Research Objectives

In this study, the hydrodynamic module for an integrated simulation tool, designed specifically for Hywind spar-type floating wind turbine, was built up in MATLAB. In order to better estimate its motion of response and validate the accuracy of both time- and frequency-domain methods, the first numerical tool contains both linear and non-linear Morison's equation. It should be noted that, by selecting the body coordinate origin at the net center of mass, including added water mass and structure mass, surge and pitch motions were decoupled. Thus, by applying the Morison's

equation, this first-order hydrodynamic simulator with high simulating speed gives a good estimation of linear response.

In order to show the importance of fully nonlinear hydrodynamics for floating wind turbine, a second numerical model was built in OrcaFlex with full QTFs input from WAMIT. WAMIT utilized panel method to mesh the structure surface and second-order potential theory to calculate hydrodynamic loading, which gave a highly accurate external loadings compared with the Morison's equation. In addition, instead of static stiffness model for mooring system, OrcaFlex solved the mooring line motion in time-domain coupled with platform motions. Thus, this fully nonlinear model shows a detailed prediction of whole floating wind turbine system and is supposed to be comparable with the experimental results in whole frequency range.

The first numerical tool in MATLAB has high adherence to classic hydrodynamic theories, making them quicker and more reliable tool for preliminary analysis of spar-type wind turbine design. The application of the Morison's equation with body-coordinated located in the net center of mass provides a new solution to spar-buoy. For detailed design of spar-type wind turbine, the second high-order model makes up for the accuracy issue in low-frequency range. It better describes the motion behavior under nonlinear wave and wind loading which is neglected by most of the existing fully coupled simulation.

2. METHODOLOGY

For offshore floating platform, there're various algorithms with high precision to evaluate the wave loading in both frequency-domain and time-domain. Although such techniques have been successfully applied to platforms working for oil and gas industry and showed a good agreement with experimental and field observations, most of the OC3 participants simply use airy wave theory together with the Morison's equation instead of a more complicated high-order hydrodynamic analysis. There're several reasons. First, current mature aerodynamic numerical analysis tools and hydrodynamic numerical tools were originally developed in two distinct conditions, including knowledge background, concerns of a problem, coding languages, et al. So it's nearly impossible to directly combine two mature numerical tools from each field through an interface program. To maintain the nonlinearity of wind load, most of the OC3 participants choose to incorporate linear wave loading into the coupled analysis for the simplicity. Second, lots of studies have validated the application of the Morison's equation to those spar platforms with small intersection area and large draft. Third, to couple a nonlinear aerodynamic module with a second-order hydrodynamic module, the simulation time will increase exponentially with dissatisfied convergence.

The study presented in this thesis starts from the widely used Morison's equation as well as linear wave theory in order to give fast simulation tools for spar-type floating wind turbine. To further meet the accuracy requirement through the whole frequency range, another model based on panel theory as well as second-order wave loading will be proposed.

2.1 The Morison's Equation

Due to the simple geometry of spar-type floaters, which can be regarded as a slender floating body, the Morison's equation has been used for external wave loading calculation. The wave-structure interaction is presented in this semi-empirical equation.

2.1.1 Frequency-domain Numerical Method

Successful application of linear frequency-domain methods to traditional oil and gas platforms throws a light on the hydro-module program for spar-type wind turbine. R/P FLIP (Floating Instrument Platform), designed and built in 1960s, is regarded as the predecessor of spar-type platform. Navigating as a ship, FLIP could flood and pitch backward for 90 degrees on the designated site. With bulkhead turning into topside, it works as a free floating spar platform to collect the oceanographic data in a certain areas. Smith and Rieder (1997) present a good paper related to FLIP, describing their frequency-domain method with an innovative coordinate. This study will follow the frequency-domain analysis of FLIP and further modify it for the specific Hywind wind turbine spar-buoy.

In present work, which focuses on the floater hydrodynamic characteristics, wave will be the first environmental loading taken into consideration. For frequency-domain method, arbitrary wave loading is decomposed into a series of wave components with single frequency, each of which could be assessed as a regular wave with a particular amplitude. Thus fluid kinematics, including displacement, velocity and acceleration, could be calculated from classic linear wave theories, correspondingly. By solving equations of motion with a series of different sinusoidal external loadings, the linear composition of results could finally present the response of structure to the irregular wave loading.

For spar-type floater in deep water, surge, pitch and heave motion attract most of the attention. In this case, due to the mooring system, heave motion with small amplitude could be neglected. Global Cartesian coordinate is set with x-axis pointing to the wave propagating direction, while the origin of body coordinate is set in the net center of mass z_c, which denotes the combination of structure mass and water added mass. Thus rotational and translational motion of this spar-type wind turbine could be uncoupled at z_c.

For the floater, its total mass and pitching moment are given by:

$$M = \int_{-H}^{h} m(z)\,dz \tag{2.1}$$

$$I = \int_{-H}^{h} \left(z - z_f\right)^2 m(z)\,dz = \gamma_f^2 M \tag{2.2}$$

where, H is the draft of spar floater, h is the height of mounted wind turbine hub, $m(z)$ is the mass distribution of spar-type wind turbine , and γ_f is the radius of gyration. The depth of structure's center of mass z_f is

$$z_f = M^{-1}\int_{-H}^{h} z m(z)\,dz \tag{2.3}$$

Since for cylinder floating body, added mass coefficient is roughly equal to 1, the depth of water added mass could be represented by the depth of water displacement z_b .

$$M_{dis} = \rho\int_{-H}^{0} A(z)\,dz \tag{2.4}$$

$$z_b = M_{dis}^{-1}\rho\int_{-H}^{0} zA(z)\,dz \tag{2.5}$$

where, $A(z) = \pi r^2(z)$ is the cross section area of the spar floater.

Thus the total mass M_i and the net center of mass, z_c , is given by

$$M_i = M + M_{dis} \tag{2.6}$$

$$z_c = \frac{1}{M_i}\left[M \cdot z_f + M_{dis} \cdot z_b\right] \tag{2.7}$$

All of this information could be accurately estimated through the design parameters for this 5MW spar-type wind turbine.

Starting from the equation of motion, forces are categorized into four terms.

(1) Fluid Inertia Term

The typical inertia term, with body coordinate originated at structure center of mass, is given by:

$$F_i(\omega) = -\rho \mathrm{C}_i \int_{-H}^{0} \left\{ g\eta_x e^{kz} + \left[\ddot{x}_f + \left(z - z_f \right) \ddot{\theta} \right] \right\} \mathrm{A}\left(z \right) dz \tag{2.8}$$

$$F_i(\omega) = -\left\{ \mathrm{C}_i \rho g \eta_x \int_{-H}^{0} e^{kz} \, \mathrm{A}\left(z \right) dz + \mathrm{C}_i \rho \int_{-H}^{0} \left[\ddot{x}_f + \left(z - z_f \right) \ddot{\theta} \right] \mathrm{A}\left(z \right) dz \right\} \tag{2.9}$$

where inertia coefficient C_i is equal to the added mass coefficient for floating body. And for nonviscous flow around a cylinder, $C_i = 1$. In addition, $\eta_x = ik\eta$ notes the complex surface slope corresponding to each frequency. Thus, the first term describes the diffraction force of wave-induced flow, while the second term is the added mass term.

Now, adopting the new body coordinate at z_c, fluid inertia term could be rewritten as:

$$F_i(\omega) = -\left[C_i \rho g \eta_x \int_{-H}^{0} e^{kz} A\left(z \right) dz + C_i \rho \int_{-H}^{0} \ddot{x}_c A\left(z \right) dz \right] \tag{2.10}$$

New radius of gyration γ_c ,

$$\gamma_c{}^2 = \frac{1}{Mi} \left[I + \left(z_f - z_c \right)^2 M + I_{dis} + \left(z_b - z_c \right)^2 M_{dis} \right] \tag{2.11}$$

(2) Drag Term

Drag force per unit area is normally with the term $-C_d \left| v\left(z \right) \right| v\left(z \right)$, which is usually substituted by a quasi-linear expression in frequency-domain method. By neglecting the phase coupling between frequency component and assuming that for small frequency solution $d\omega$, velocity magnitude $\left| v\left(z \right) \right|$ is roughly equal to the total root mean square, the nonlinear term could be written as:

$$D_v\left(z \right) = C_d \cdot V\left(z \right) \tag{2.12}$$

wherer C_d is the drag coefficient and $V(z)$ is the root mean square velocity of fluid relative to the structure, which can be calculated from the wave elevation spectrum.

$$V\left(z \right) \approx \sqrt{\int_0^\infty \eta\left(\omega \right)^2 \omega^2 e^{2k(\omega)z} d\omega} \tag{2.13}$$

Thus the drag force term is given by:

$$F_d(\omega) = 2\pi\rho\int_{-H}^{0}\left\{\frac{\omega\eta_x}{ik}e^{kz} - \left[\dot{x} + (z - z_c)\dot{\theta}\right]\right\}D_v(z)r(z)dz \tag{2.14}$$

where the relative velocity between fluid and moving structure is given.

(3) Restoring Term

The restoring term consist of two parts, hydrostatic moment for pitch and restoring force and moment from mooring system.

Hydrostatic restoring moment for pitch is given by:

$$M_b = -\frac{\pi}{64}\rho g D^4\theta - Mg\overline{GB}\theta \tag{2.15}$$

The restoring force and moment provided by mooring system is given by:

$$F_{sp} = -K_x\left(x_c - \overline{FC}\theta\right) \tag{2.16}$$

$$M_{sp} = -K_x\left(x_c - \overline{FC}\theta\right)\overline{FC} - \left(M_{dis} - M\right)g\overline{FC}\theta \tag{2.17}$$

where $\overline{GB}$ is the distance between structure mass center and buoyancy center, $\overline{FC}$ is the distance between the fairlead F and the body coordinate origin, and K_x is the mooring stiffness with respect to the offset along x-axis.

(4) Wave Forces

Based on the linear wave theory, regular wave force in deep water is

$$F_p(\omega) = -\rho g\eta_x\int_{-H}^{0}e^{kz}A(z)dz \tag{2.18}$$

(5) Final Equations

For the net force, according to Newton's Second Law, we have,

$$M_i\ddot{x}_c = F_i(\omega) + F_d(\omega) + F_{sp} + F_p(\omega) \tag{2.19}$$

Substitute each term of the equation,

$$M_i \ddot{x}_c = -\left(1+C_i\right)\rho g \eta_x \int_{-H}^{0} e^{kz} A\left(z\right) dz - i \cdot 2\pi\rho g \frac{\eta_x}{\omega} \int_{-H}^{0} e^{kz} D_v\left(z\right) r\left(z\right) dz \quad (2.20)$$

$$-\left[2\pi\rho \int_{-H}^{0} D_v\left(z\right) r\left(z\right) dz\right] \dot{x}_c - \left[2\pi\rho \int_{-H}^{0} \left(z - z_c\right) D_v\left(z\right) r\left(z\right) dz\right] \dot{\theta} - \mathrm{K}_x \cdot x_c + \mathrm{K}_x \cdot \overline{FC}\theta \quad (2.21)$$

Assume that the surge and pitch motion is proportional to the form $e^{i\omega t}$, the final equation for horizontal net force could be written as:

$$\left(-M_i\omega^2 - i\omega C_1 + K_x\right) x_c + \left(-i\omega C_2 - K_x \overline{FC}\right)\theta = -F_\omega \eta_x \quad (2.22)$$

where,

$$F_\omega = \rho g \left[\left(1+C_i\right) \int_{-H}^{0} e^{kz} A\left(z\right) dz + i \cdot \frac{2\pi}{\omega} \int_{-H}^{0} e^{kz} D_v\left(z\right) r\left(z\right) dz\right] \quad (2.23)$$

$$C_1 = 2\pi\rho \int_{-H}^{0} D_v\left(z\right) r\left(z\right) dz \quad (2.24)$$

$$C_2 = 2\pi\rho \int_{-H}^{0} \left(z - z_c\right) D_v\left(z\right) r\left(z\right) dz \quad (2.25)$$

For the net moment, each force term should be added with $\left(z - z_c\right)$ in the integral, and hydrostatic restoring moment for pitch is an extra term for net moment equation. Thus we have,

$$\left(-i\omega D_1 + \mathrm{K}_x \overline{FC}\right) \mathrm{x}_c + \left(-\omega^2 \mathrm{M}_i \gamma^2{}_c - i\omega D_2 - K_\theta\right)\theta = -\eta_x T_w \quad (2.26)$$

where

$$T_\omega = \rho g \left[\left(1+C_i\right) \int_{-H}^{0} e^{kz} A\left(z\right) \left(\mathrm{z} - \mathrm{z}_c\right) dz + i \cdot \frac{2\pi}{\omega} \int_{-H}^{0} e^{kz} D_v\left(z\right) r\left(z\right) \left(\mathrm{z} - \mathrm{z}_c\right) dz\right] \quad (2.27)$$

$$D_1 = 2\pi\rho \int_{-H}^{0} D_v\left(z\right) r\left(z\right) \left(\mathrm{z} - \mathrm{z}_c\right) dz \quad (2.28)$$

$$D_2 = 2\pi\rho \int_{-H}^{0} \left(z - z_c\right)^2 D_v\left(z\right) r\left(z\right) dz \quad (2.29)$$

$$K_{SH} = \frac{\pi}{64} \rho g D^4 + Mg\overline{GB} \quad (2.30)$$

$$K_\theta = K_x \overline{FC}^2 - \left[\left(M - M_{dis}\right) g \overline{FC} + K_{SH}\right] \quad (2.31)$$

2.1.2 Time-domain Numerical Method

For better coupling with the aerodynamic calculation module, which deals with most of the nonlinear wind loads, simulating the floater motion in time-domain is widely adopted during recent years. For the forces and moments working on the moving structure, the physical meaning of each term is identical to the frequency-domain method. However, the original term for drag force is remained, in order to show the nonlinearity of viscous force.

In presented work, Newmark-β Method is applied to undergo an iterative calculation for structure kinematics with the increment of each time step. With given mass term and restoring term, damping term is regarded as external viscous force put together with wave forces. Thus, the main problem to be solved is getting wave loading time series from the input wave elevation. For frequency-domain method, after decoupling the wave components corresponding to each frequency, classic linear wave theory is used for fluid kinematics, which could be directly substitutes into the wave force equations. However, for irregular wave elevation time series, such derivation is invalid and time filter for convolution and stretching are needed. Wheeler (1970) published a classic paper related to method for calculating forces produced by irregular waves.

The wave forces on cylinder body could be accurately expressed by Morison's Equation,

$$F(z,t) = C_m \frac{\pi \rho D^2}{4g} \frac{du}{dt} + C_d \frac{\rho}{2g} D|u|u \tag{2.32}$$

So, Wheeler's method is used to find information of fluid velocity and acceleration based on the wave elevation time series. Based on the small-amplitude wave theory, we have

$$\eta(\mathrm{t},\mathrm{x}) = A\cos\theta \tag{2.33}$$

$$u(\mathrm{t},\mathrm{z}) = \omega \cdot \frac{\cosh\left[k(z+d)\right]}{\sinh(kd)} A\cos\theta = \omega \cdot G_s(\mathrm{z},d,\mathrm{k}) \cdot \eta(t) \tag{2.34}$$

where $G_s(z,d,k)=\dfrac{\cosh\left[k(z+d)\right]}{\sinh(kd)}$

Thus, by applying Fourier analysis, a series of regular wave time series is chosen to represent the irregular wave,

$$\eta(t)=\sum_n A_n\cos(\omega_n t-\phi_n) \tag{2.35}$$

$$u(t,z)=\sum_n \omega_n G_s(z,d,k_n)A_n\cos(\omega_n t-\phi_n) \tag{2.36}$$

Here, by assuming that each component with a specific frequency produce the fluid velocity independently, convolution with the impulsive-response function $h(\tau,z)$ is adopted to build up a time filter.

$$u(t,z)=\int_{-\infty}^{\infty} h(\tau,z)\eta(\mathrm{t}-\tau)d\tau \tag{2.37}$$

$$h(\tau,z)=2\int_{-\infty}^{\infty}\omega G_s\cos(\omega\tau)df \tag{2.38}$$

By discretizing the equations above, the numerical forms are given:

$$u(N\Delta t,z)=\Delta\tau\sum_{j=-M}^{M} h(j\Delta\tau,z,d)\eta(N\Delta t-j\Delta\tau) \tag{2.39}$$

$$h(j\Delta\tau,z,d)=2\int_0^{\infty}2\pi fG(z,d,L)\cos(2\pi fj\Delta\tau)df \tag{2.40}$$

where N denotes the time point for wave elevation time series, and j denotes the point for time filter with a length of (2M+1).

With this numerical time filter, for the Nth time point of wave elevation time series, its velocity could be represented by the time points from (N-M) to (N+M), by timing the coefficient of corresponding points in the time filter. The acceleration of fluid is given by the central difference method. Thus the time series of wave loading could be well expressed by them. With this wave loading time series as input, Newmark-β Method is really straightforward to continue the rest of computation in time-domain to have the surge and pitch motion time series. Following is the brief steps of algorithm on Newmark-β Method.

Step1 The mass matrix $[M]$, the damping matrix $[C]$, the stiffness matrix $[K]$, and the initial conditions of displacement $[X_0]$ and velocity $[\dot{X}_0]$ are given as initial input.

Step2 The time series of force vector $\{F(t)\}$ is calculated according to the method stated above.

Step3 The initial acceleration is given as below:

$$\{\ddot{X}_0\} = \frac{1}{M}\left(F_0 - C\dot{X}_0 - KX_0\right) \tag{2.41}$$

Step4 $\delta = 0.5$, $\beta = 0.25\times(0.5+\delta)^2$ and the constant coefficients are listed as below:

$$\begin{aligned} &a_0 = \frac{1}{\beta\Delta t^2}, a_1 = \frac{\delta}{\beta\Delta t}, a_2 = \frac{1}{\beta\Delta t}, a_3 = \frac{1}{2\beta} - 1 \\ &a_4 = \frac{\delta}{\beta} - 1, a_5 = \frac{\Delta t}{2}\left(\frac{\delta}{\beta} - 2\right), a_6 = \Delta t(1-\delta), a_7 = \delta\Delta t \end{aligned} \tag{2.42}$$

where Δt is the time step.

Step5 The equivalent coefficient $\hat{K}$ is given by:

$$\hat{K} = K + a_0 M + a_1 C \tag{2.43}$$

It should be noted that this $\hat{K}$ is a coefficient for numerical calculation, which is totally different from the original stiffness matrix $[K]$.

Step6 The linear combinations of displacement, velocity, and acceleration to calculate motion in next time step are as follow:

$$\begin{aligned} &\hat{F}_{t+\Delta t} = F_{t+\Delta t} + M\left(a_0 X_t + a_2\dot{X}_t + a_3\ddot{X}_t\right) + C\left(a_1 X_t + a_4\dot{X}_t + a_5\ddot{X}_t\right) \\ &X_{t+\Delta t} = \hat{K}^{-1}\hat{F}_{t+\Delta t} \\ &\ddot{X}_{t+\Delta t} = a_0\left(X_{t+\Delta t} - X_t\right) - a_2\dot{X}_t - a_3\ddot{X}_t \\ &\dot{X}_{t+\Delta t} = \dot{X}_t + a_6\ddot{X}_t + a_7\ddot{X}_{t+\Delta t} \end{aligned} \tag{2.44}$$

Step7 For each time step, external wave force of next step $F_{t+\Delta t}$ is calculated by $X_t, \dot{X}_t, \ddot{X}_t$ and compared with the time series $\{F(t)\}$ in step 2. The convergence has to achieve 0.1% in order to move to the next time step.

2.2 Second-order Wave Theory

Even though linear wave theory and the Morison's equation is widely applied to the offshore platform analysis in frequency-domain, the high-order hydrodynamic loads acting on floating platforms may bring about several important impact. For example, for slacked-moored floaters, it may drift slowly with a large period, due to the mean-drift loads know as difference-frequency loads. Whereas, for taut-moored structures, like Tension Leg Platform (TLP) or fixed-bottom monopile, they may suffer ringing effects, which are mainly from the sum-frequency loads. For numerical model based on linear wave theory, even though the simulation time is largely reduced, some important hydrodynamic response listed above may also be neglected.

For floating wind turbine system, some studies of OC3 participants, like FAST predictions mentioned above, have already showed the limitation of linear wave theory and the Morison's equation in low frequency range. However, for floating wind turbine system, experimental results indicate the importance of second-order loading, including both aerodynamic and hydrodynamic ones. Thus, in order to eliminate the difference between experimental results and numerical predictions out of the wave-frequency range, a third model based on the panel theory for hydrodynamic loading will take high-order wave loading into consideration.

Normally second-order wave loading could be linearly superimposed with the first order one. Because of the linear assumption adopted in frequency-domain analysis, high-order hydrodynamic analysis is mostly base on time-domain method, so that nonlinearity can be better preserved. The equation of motion in time domain is given by Cummins (1962) as follow.

$$\left(M + A_{\infty}\right)\ddot{X} + \int_0^t K\left(t-\tau\right)\dot{X}\left(\tau\right)d\tau + C_{hydro}X = F_{wave}^{(1)} + F_{wave}^{(2)} \tag{2.45}$$

where M is the mass matrix, A_{∞} is the added-mass matrix, K is the retardation matrix, C_{hydro} is the hydrostatic stiffness matrix, and $F_{wave}^{(1)}, F_{wave}^{(2)}$ represent first-order and second-order wave loading respectively.

First-order wave loading is calculated for each single regular wave, which is

$$F_{wave}{}^{(1)}_{i} = \mathrm{Re}\left(AH_i e^{j\omega t}\right), i = 1,2,...6 \tag{2.46}$$

where i represents the six degree of freedom, j denotes the imaginary number $\sqrt{-1}$, A is the amplitude of each single regular wave with a certain period, and H is the first-order wave loads per unit amplitude (RAOs). Thus for a series of irregular wave, with the help of Fast Fourier Transform (FFT), the first-order wave loading is

$$F_{wave}{}^{(1)}_{i} = \sum_{k=1}^{N} \mathrm{Re}\left(A_k H_i\left(\omega_k\right) e^{j\omega_k t}\right), i = 1,2,...6, \omega_k = \left(k-1\right)\delta\omega \tag{2.47}$$

Similarly, second-order wave loading can also be frequency independent and represented as the superimposition of incoming regular waves. Duarte and Sarmento (2014) give the theoretical derivation of second-order hydrodynamic forces on floating wind turbine in details. Different from first-order wave loading, it is always calculated in pairs and divided into the contributions from sum- and difference-frequency respectively. For a pair of waves, whose amplitudes are A_k and A_l with wave frequencies ω_k and ω_l correspondingly, the second-order part of its hydrodynamic loadings could be written as

$$F_{wave}{}^{(2)}_{i} = \mathrm{Re}\left(\sum_{k=1}^{N}\sum_{l=1}^{N}\left[A_k A_l H_i^{+}\left(\omega_k,\omega_l\right)e^{j(\omega_k+\omega_l)t} + A_k A_l^{*} H_i^{-}\left(\omega_k,\omega_l\right)e^{j(\omega_k-\omega_l)t}\right]\right) \tag{2.48}$$
$$i = 1,2,...6$$

where $*$ denotes the complex conjugate, $H_i^{+}\left(\omega_k,\omega_l\right)$ and $H_i^{-}\left(\omega_k,\omega_l\right)$ are two different quadratic transfer functions (QTFs) for sum- and difference-frequency effects corresponding to the i^{th} degree of freedom.

For QTF matrices, the following symmetry relations can be well applied to reduce the computational effort.

$$\begin{aligned} H_i^{+}\left(\omega_k,\omega_l\right) &= H_i^{+}\left(\omega_l,\omega_k\right) \\ H_i^{-}\left(\omega_k,\omega_l\right) &= H_i^{-}\left(\omega_l,\omega_k\right)^{*} \end{aligned} \tag{2.49}$$

In equation (2.48), there's a constant term arising from the quadratic interaction between first-order wave loading terms, which doesn't ask for second-order wave

potential. It is called mean-drift loading, because it equals the average of second-order wave loads. Mean-drift force can be calculated as follow,

$$F_{wave}{}^{(Drift)}_{i} = \mathrm{Re}\left(\sum_{k=1}^{N} A_k A_k^{*} H_i^{Drift}\left(\omega_k\right)\right), i = 1,2,...6 \tag{2.50}$$

Since it takes huge effort to calculate full QTF matrices and double summation in equation (2.48), Newman's approximation in time-domain is widely adopted for difference-frequency effect. It assumes that, for a pair of waves A_k and A_l, if the values of their frequencies ω_k and ω_l are close enough, the slow-drift loading can be presented by the mean-drift terms calculated from the first-order solution. Thus, for platforms with large natural periods, this method has been proved to be simple and useful. Newman's approximation is given as follow,

$$F_{wave}{}^{(-)(2)}_{i} = \left[\mathrm{Re}\left(\sum_{k=1}^{N} A_k \sqrt{2H_i^{-}\left(\omega_k,\omega_k\right)} e^{j\omega_k t}\right)\right]^2\Bigg|_{H_i^{-}(\omega_k,\omega_k)\geq 0} - \left[\mathrm{Re}\left(\sum_{k=1}^{N} A_k \sqrt{-2H_i^{-}\left(\omega_k,\omega_k\right)} e^{j\omega_k t}\right)\right]^2\Bigg|_{H_i^{-}(\omega_k,\omega_k)<0}$$
$$i = 1,2,...6 \tag{2.51}$$

Due to the basic assumption of Newman's approximation, in QTF matrices, the near-diagonal terms should be carefully estimated while the far-diagonal terms are of much less value, since it exerts little effect on platform with large inertia. Thus, for narrow-banded spectrum, it turns out to be a good approximation for second-order wave loads.

However, one should notice that for higher accuracy and wider application, full QTFs are preferable, especially for wide-band wave spectrum or platforms working in shallow water areas. In these cases, off-diagonal terms in the QTF matrices are unneglectable.

3. LINEARIZED NUMERICAL MODELS

Airy wave theory and the Morison's equation are widely used for first-order hydrodynamic analysis of spar-type platform. The first part of this study starts from these theories and gives a quick first-order numerical simulation tool in frequency-domain and time-domain respectively.

3.1 5MW Baseline OC3-Hywind Wind Turbine

NREL (2010) published the definition of the floating system for phase IV. 5MW baseline wind turbine, as a representative utility-scale, multi-megawatt turbine, has been used for reference model in several upwind wind turbine research programs. The tower properties and blade properties have been modified by NREL and provided to all the OC3 participants. As to the Hywind spar-type floater, which was originally designed by Statoil, together with a three-line mooring system, the detailed design is also publicly available.

However, given the limitation of experimental installation under a 1:50 scale, experimental set-up always has to make several adjustment. The experimental data adopted as reference in this study is from State Key Lab of Ocean Engineering at Shanghai Jiao Tong University by Duan et al (2015). For the wind turbine model, even though they spare every effort to select light materials and match the properties of blade and tower well, the installation of recording instrument adds around 25% more weight on the upper part. The detailed comparison between designed wind turbine and its experimental counterpart is given in table 3.1. Note that CM locations are calculated from still water level (SWL).

For the spar-type floater, the main dimensions of platform model is strictly manufactured according to the given design data. But in order to make the whole floating system perfectly match the designed one, model platform has lighter weight in full scale to balance the extra weight from wind turbine. The property of platform is given in table 3.2 and its main dimension is given in figure 3.1.

It should be noted that, in order to testify the feasibility of numerical models in this study, all the input for numerical simulations adopted the experimental values measured for full scale.

Table 3.1 Properties of NERL 5-MW Baseline Wind Turbine (Duan et al, 2015)

	NREL Design		Experimental Modification	
Item	Mass(kg)	Center of Mass(m)	Mass(kg)	Center of Mass(m)
Blade (three in total)	53,220	90	52,659	90.65
Hub	56,780	90.17	57,272	90.65
Nacelle	240,000	89.35	232,291	90.65
Tower	249,718	43.4	287,128	51
4 Markers at Tower Bottom	-	-	27,163	39.9
1 Marker at Nacelle	-	-	6,791	92.15
Data Cables	-	-	86,228	57.1
Total Wind Turbine	599,718	70.35	749,532	69.45

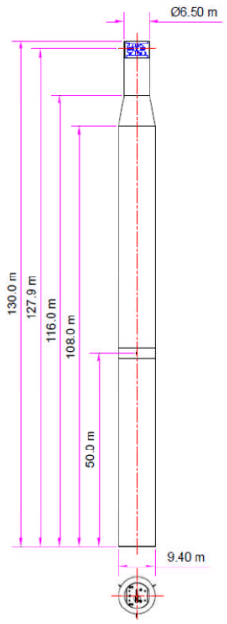

Figure 3.1 Main dimensions of Hywind floater (Duan et al, 2015)

Table 3.2 Properties of Spar-type Platform (Duan et al, 2015)

Item	Unit	Design	Experiment
Platform mass (with ballast)	kg	7,466,330	7,316,578
Draft	m	120	120
CM location	m	-89.92	-94.1495
Platform roll inertia about CM	$kg \cdot m^2$	4,229,230,000	4,656,382,813
Platform pitch inertia about CM	$kg \cdot m^2$	4,229,230,000	4,656,382,813

In the wave basin test, 200 meter water depth was modeled and a taut three-line mooring system with a special delta connection (shown in figure 2.2) was simulated. Tension in the three lines was measured by sensors located in the joints of three lines, which is noted as A in the figure 3.2. The properties of whole mooring system are well modeled with detailed design given by table 3.3.

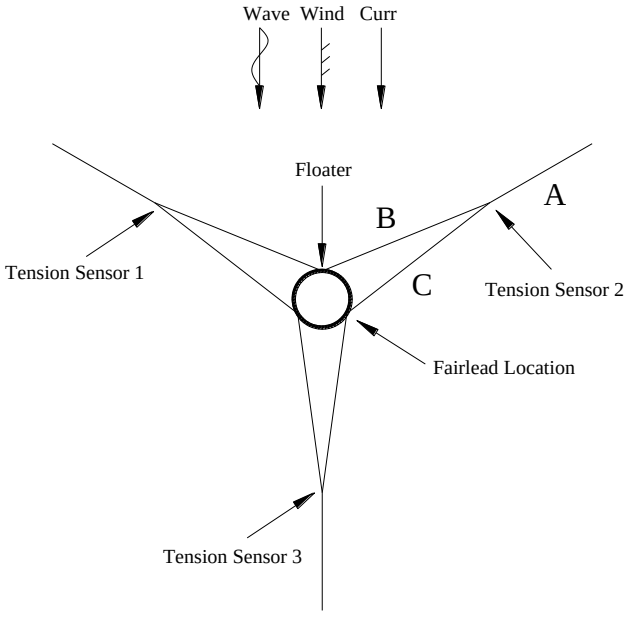

Figure 3.2 Layout of mooring system (Duan et al, 2015)

Table 3.3 Mooring System Properties (Duan et al, 2015)

Item	Unit	Value
Number of mooring lines		3 for A; 6 for B&C
Angle of two mooring lines of type A	deg	120
Anchor radius	m	445
Anchor depth below SWL (water depth)	m	200
Radius of fairlead	m	5.2
Fairlead depth below SWL	m	70
Unstretched line length A	m	424.35
Unstretched line length B&C	m	30
Line A diameter	m	0.167
Line B&C diameter	m	0.125
Mass per length line A (dry)	kg/m	22.5
Mass per length line B&C (dry)	kg/m	12.6
Mass per length line A,B&C (wet)	kg/m	0
Axial stiffness line A (EA)	N	121,000,000
Axial stiffness line B&C (EA)	N	68,000,000

In sum, the whole set-up of 5MW baseline OC3 Hywind wind turbine system was modeled in the wave basin according to the design published by NREL. Table 3.4 shows the overall comparison between design and experiment.

Table 3.4 Properties of Entire Floating System (Duan et al, 2015)

Item	Unit	Design	Experiment
Total mass	kg	8,066,048	8,066,110
Center of mass	m	-78	-78.95
Platform roll/pitch inertia about overall CM	$kg \cdot m^2$	-	23,161,872,557
Pretension of each mooring line	kN	-	2762.375

For spar platform working under unidirectional wave, motions of surge, pitch and heave attract most of the attention due to their relatively large response amplitudes. But for OC3 Hywind spar-type floater, which has a deep draft as well as large displacement, heave motion is highly damped. Thus the preliminary spectral analysis of experimental data mainly focuses on the surge and pitch motions.

SKLOE conducted a series of system identification tests to guarantee that the floating wind turbine system model well match the design physical property parameters, including mass and inertia of moment, natural periods, system stiffness, total system damping, and linear response characteristics RAOs. Figure 3.3 and figure 3.4 shows the surge and pitch motion spectra under white noise wave with 2 meters wave height. According to the peak frequencies shown in the figures, natural periods of the structure for surge and pitch are 0.024Hz and 0.029Hz respectively.

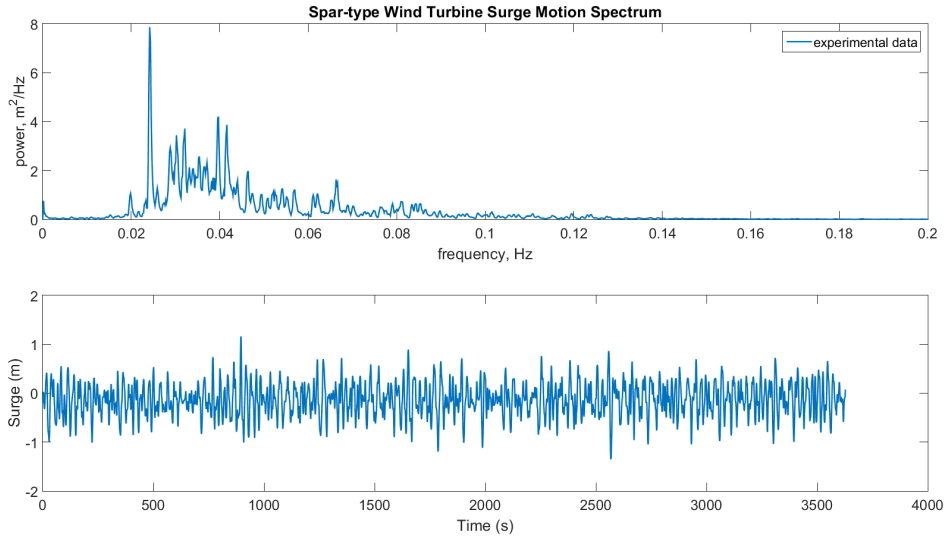

Figure 3.3 Surge motion spectrum under white noise with wave height H=2m

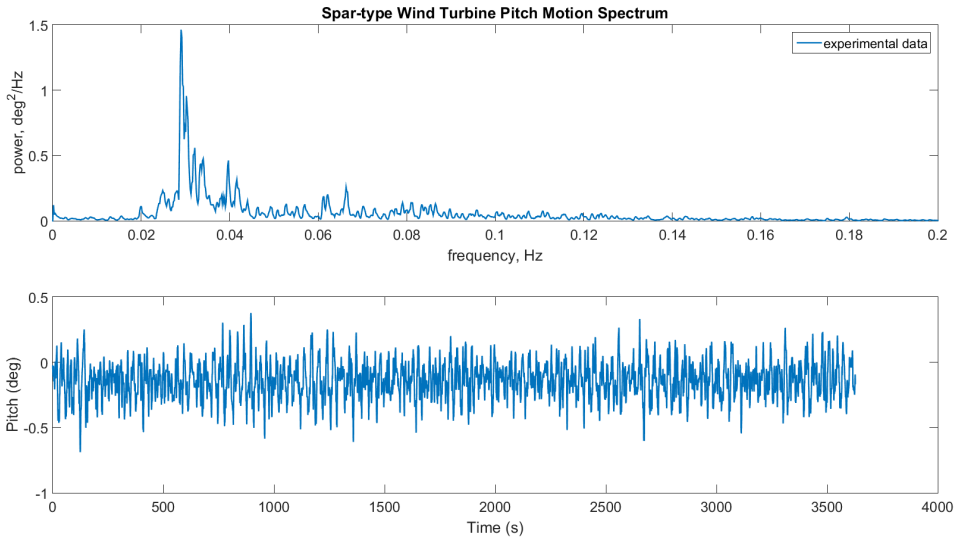

Figure 3.4 Pitch motion spectrum under white noise with wave height H=2m

In the presented thesis, environmental conditions with irregular wave (JONSWAP spectrum, $H_s = 7.1m, T_p = 12.1s, \gamma = 2.2$), no current and no wind are selected to test the hydrodynamic accuracy of numerical models. The input wave spectrum and corresponding time series are shown in figure 3.5. The surge and pitch motions time series of floating wind turbine system with parked blade were recorded and shown in figure 3.6 and figure 3.7, together with their spectral analysis results. It should be noted that all the 6 DOF motions in the experiment are recorded with respect to SWL.

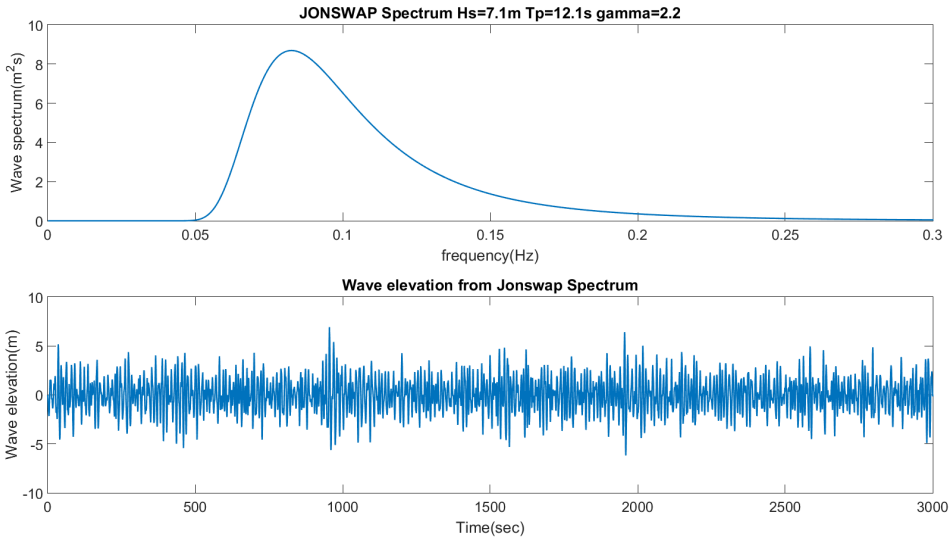

Figure 3.5 JONSWAP Spectrum and the corresponding time series for irregular wave with Hs=7.1m, Tp=2.2s, gamma=2

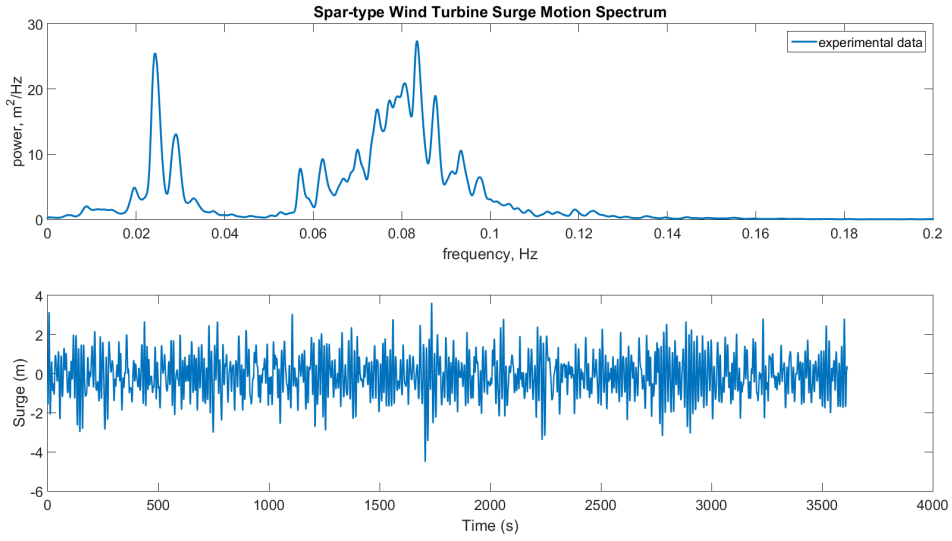

Figure 3.6 Experimental data and motion spectrum of surge motion for JONSWAP Spectrum Hs=7.1m, Tp=2.2s, gamma=2

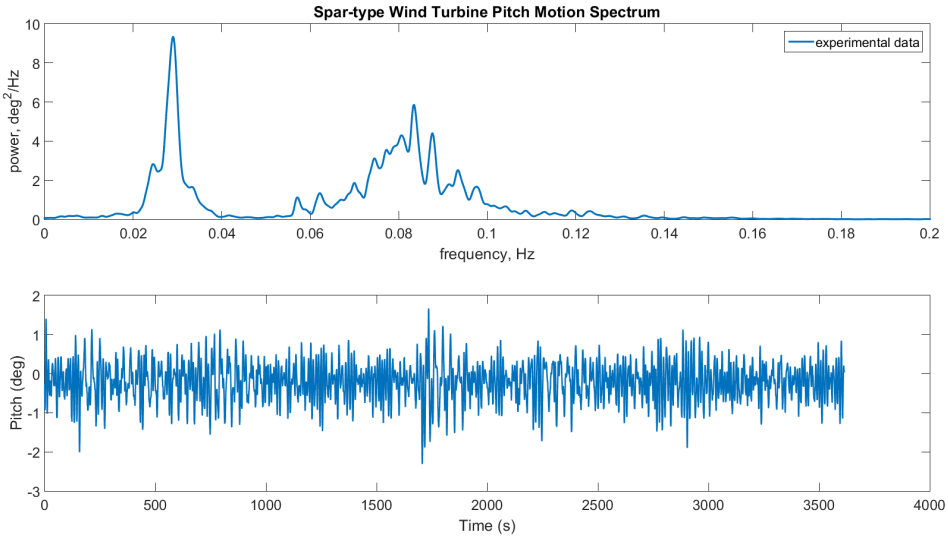

Figure 3.7 Experimental data and motion spectrum of pitch motion for JONSWAP Spectrum Hs=7.1m, Tp=2.2s, gamma=2

For figure 3.6, except for the peak in wave-frequency range 0.08355 Hz, which is corresponding to the wave peak frequency 0.083 Hz, there're another two peaks in low-frequency range with values of 0.02417 Hz and 0.029 Hz. Same phenomenon goes for pitch spectrum in figure 3.7 that low-frequency range has a main peak with frequency 0.02918 Hz and a small one with frequency 0.02451 Hz. Taking natural frequencies measured in white noise wave basin tests as a reference, one can easily figure out the coupling effect between surge and pitch motions. In addition, by comparing the spectrum areas located in low-frequency range and wave-frequency range, it can be concluded that motion response in low-frequency range plays an important role in the hydrodynamic analysis for Hywind spar-type floater. All the predictions made by the following two numerical models will be compared with these experimental results later.

3.2 Frequency-domain Numerical Model

Based on the Morison's equation in frequency-domain, the first model based on first-order wave loading is derived. The process for frequency-domain calculation is quite straightforward which could be divided into two steps: 1) to calculate external loadings for each incoming single regular wave with a certain wave amplitude and period and substitute into the equation of motion for the numerical solver; 2) to linearly superimpose all the response components. By following the methodology stated previously, there're several ideas needed to be specially illustrated in the process of building up frequency-domain numerical model.

First, different form the traditional potential wave theory, the Morison's equation takes drag force into consideration by introducing drag force coefficient C_d. However, the C_d values for a cylinder are always determined by the measured curve with respect to the Reynold's number, which may vary according to the floating body shape. Thus, for each cylinder body element, divided along the vertical direction, C_d values should be selected carefully based on roughly estimated Re. In addition, the expression of drag force term brings about second-order results which cannot be directly applied to the frequency-domain model. It should be noted that, since the motion amplitudes of structure is relatively small compared with the fluid velocity in a mild sea state, it is acceptable to directly use absolute fluid velocity instead of absolute relative velocity between structure and fluid to have a vertical-direction varying damping coefficient for first-order wave loading estimation. So equation (2.12) shows the idea to linearize the drag force term by simplifying the absolute value of fluid velocity $v(z)$ into $V(z)$, which is the root mean square value of fluid velocity. Thus $V(z)$ is no longer related to frequency but only a function with variable z. Dependent on the assumptions for such linearization, it is only feasible for structure with small amplitude of motion and the analysis in the frequency-domain with small frequency solution.

Second, for spar-type platform with large draft, like Hywind, the coupling effect between surge and pitch motion could not be neglected, as shown in the experimental

figures above. To simplify the solver and reduce the calculating effort, the presented study adopted an innovative coordinate published by the researchers of FLIP. The origin of such innovative coordinate will be set on the rotation center, where there's only pure rotation without any horizontal motions. For slender floating body like spar-platform, they proved that with wave frequency increasing beyond a certain range, such rotation center tended to locate in the net mass center, which includes the total weight of structure and its added mass. And since this first numerical model is expected to provide loading only in wave-frequency range, this new type of body-coordinate is expected to be feasible and of higher calculating efficiency. Figure 3.8 proves this relationship between rotation center depth and wave frequency, with data from the experimental case. Thus in the calculation of frequency-domain model, net mass center is selected as new origin for body-doordinate.

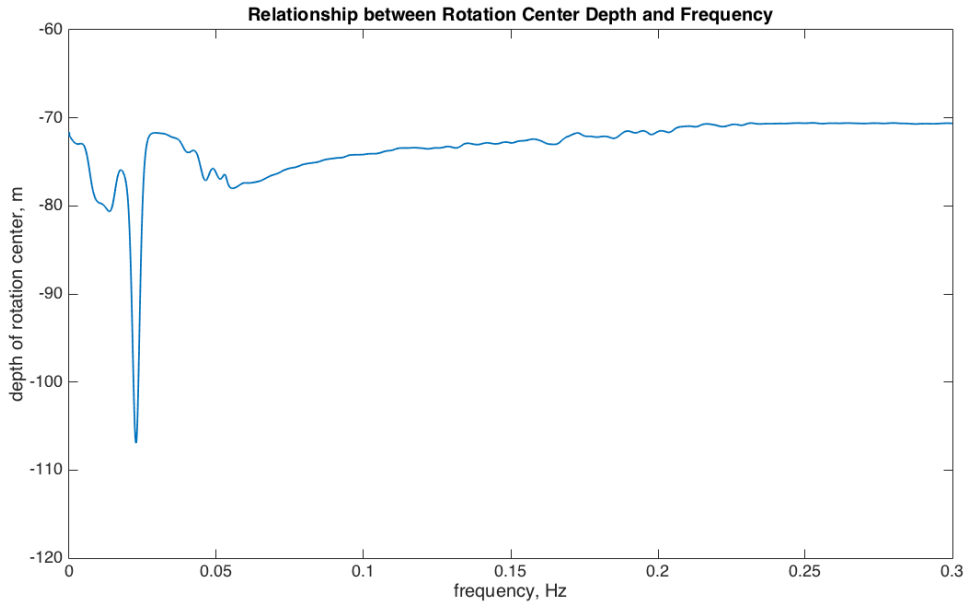

Figure 3.8 Relationship between rotation center depth and frequency for JONSWAP Spectrum Hs=7.1m, Tp=2.2s, gamma=2

Third, for the mooring system, a static stiffness model is used to be equivalent with the stiffness of designed mooring lines. The static offset tests were conducted by SKLOE so that the measured curve for the horizontal stiffness of mooring system along surge direction is going to provide mooring stiffness value, which is roughly 400 KN/m. Figure 3.9 gives the measured horizontal restoring stiffness.

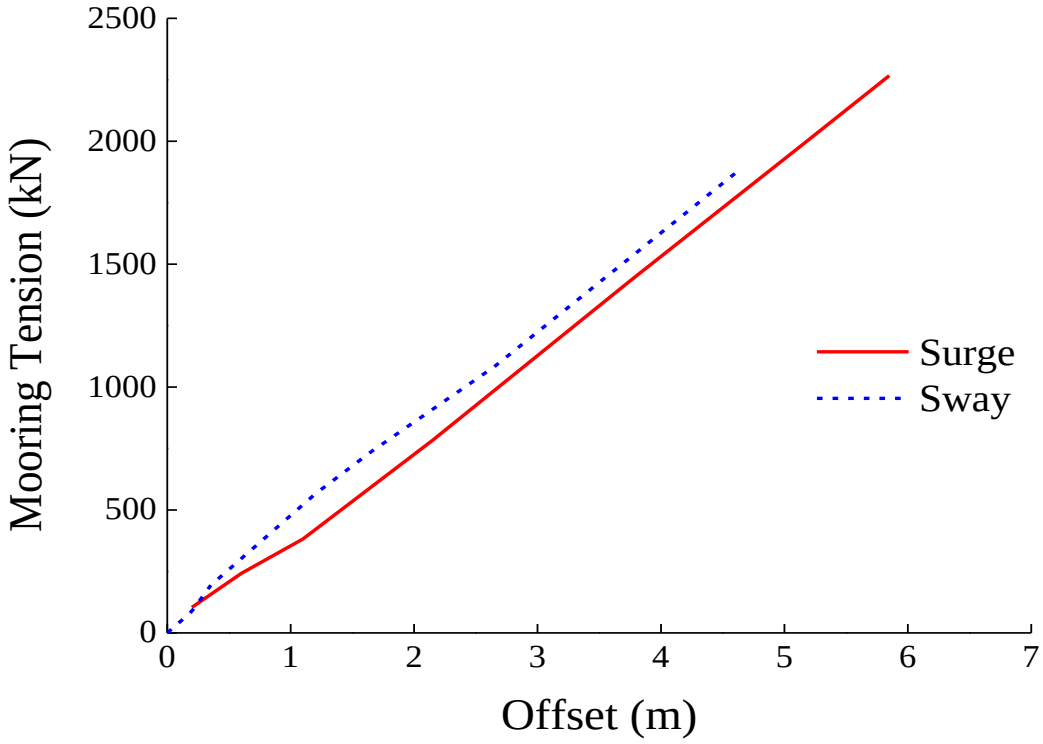

Figure 3.9 Experimental results of mooring horizontal restoring stiffness (Duan et al, 2015)

Based on the methodology presented above, frequency-domain model derived from linear wave theory and the Morison's equation is built in MATLAB. Coding of this model is attached in Appendix. Using the example case selected before as reference, the numerical results given by this model are shown in figure 3.10 and figure 3.11. Due to the selection of new body coordinate, the surge and pitch motion of body-coordinate

origin will be first given, as shown in figure 3.10. Then the surge motion on SWL could be calculated by superimposing the surge of origin with the coupled surge motion on water surface from pitch motion.

Noted that the real rotation center of platform is not exactly same as the net mass center, which is chosen to be the body-coordinate origin. So the surge amplitude of the origin is not exactly equal to zero but a small value. Compared with the experimental data, predicted surge motion given by frequency-domain model matches it very well in frequency-domain range. However, for the peak in low-frequency range, it hardly shows any information, due to the theoretical limitation of Airy wave theory and the Morison's equation.

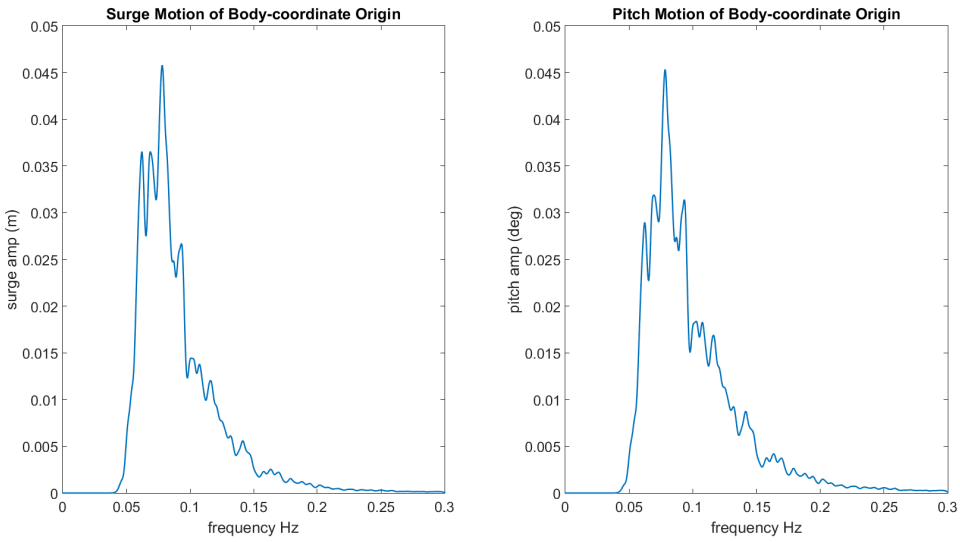

Figure 3.10 Surge and pitch motion amplitude of body-coordinate origin

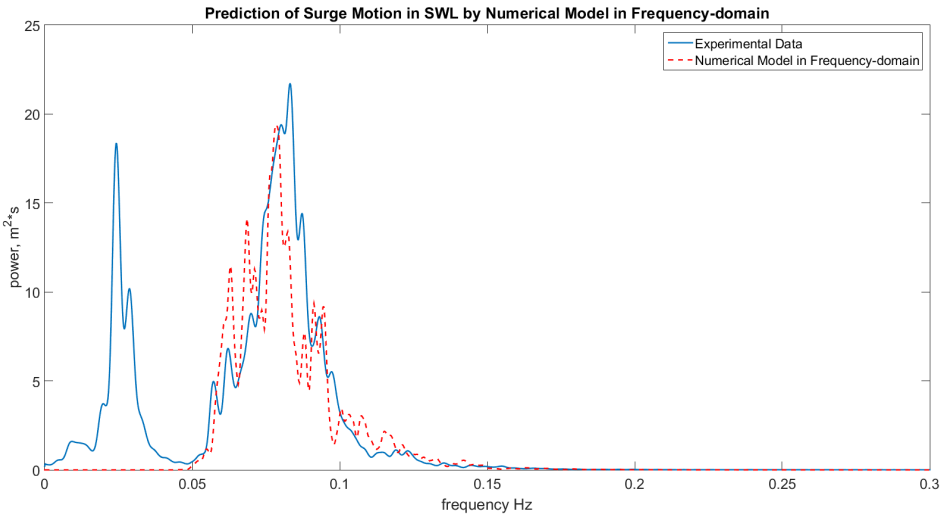

Figure 3.11 Surge motion spectrum on SWL compared with experimental data

3.3 Time-domain Numerical Model

For time-domain numerical model, it applies same theoretical basis with frequency-domain one. The main difference is about the calculation of external force terms and the numerical method to solve equation of motion by time-domain iteration.

First, since time-domain solution starts from the initial conditions, including displacement, velocity and acceleration, and updates all of them for each time-step, the external force terms should be given in time series. For irregular wave train, the methodology of acquiring its corresponding wave force time series is presented in the previous section. In addition, the external force of each step should be regarded as an impulsive force which will have time-delay effect, so that convolution is needed. And for numerical calculation, a Wheeler stretching filter is selected to play the same role as convolution discretely, shown in equation (2.37-2.40). Figure 3.12 gives the shape of time filter used in this time-domain model, which can directly calculate the velocity and acceleration from the given elevation of a series of irregular wave. Since wave elevation varies with water depth, the time filter will also have different shapes with respect to water depths. Figure 3.13 and 3.14 show the results of calculated fluid velocity and

acceleration of the selected experimental case. These results will be substituted into the Morison's equation for external wave loadings, as shown in figure 3.15 and figure 3.16.

Second, for the time-domain solver, one of the most outstanding advantages is to compare with the recorded time series of motions. However, due to the lack of original wave elevation time series measured in front of the wave paddle, the initial phase information cannot be determined. So calculated time series from time-domain model is not able to compare with the experimental recorded one. Here, spectra of response motion is used instead in figure 3.17.

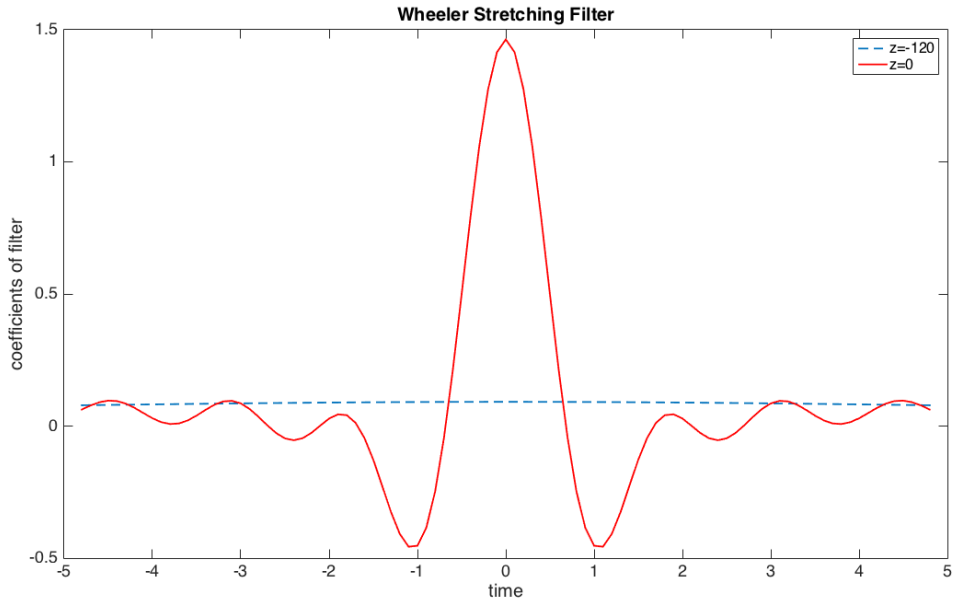

Figure 3.12 Wheeler stretching filter for still water level and bottom of platform

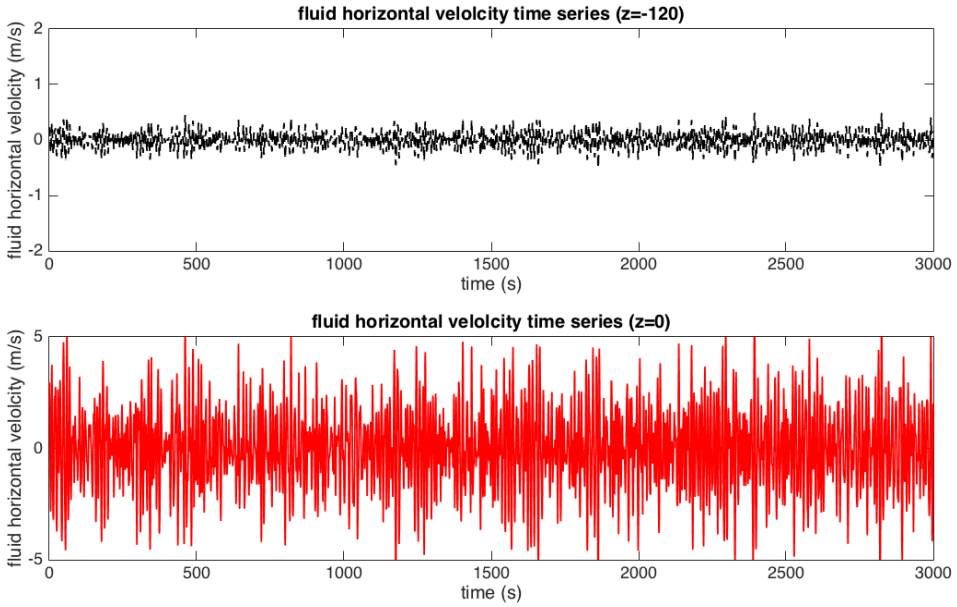

Figure 3.13 Fluid velocity calculated from wave elevation of irregular wave with JONSWAP Spectrum Hs=7.1m, Tp=2.2s, gamma=2

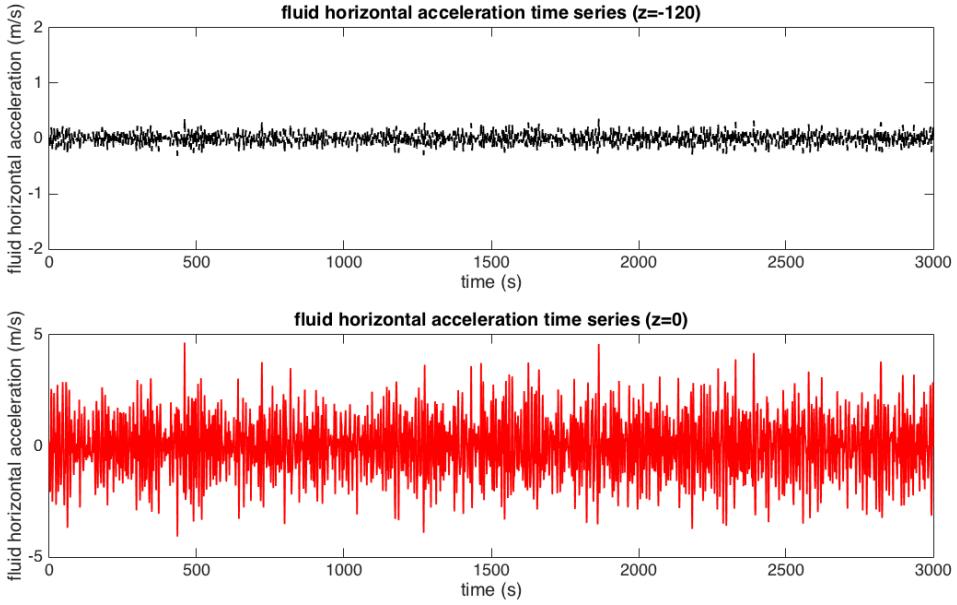

Figure 3.14 Fluid acceleration calculated from wave elevation of irregular wave with JONSWAP Spectrum Hs=7.1m, Tp=2.2s, gamma=2

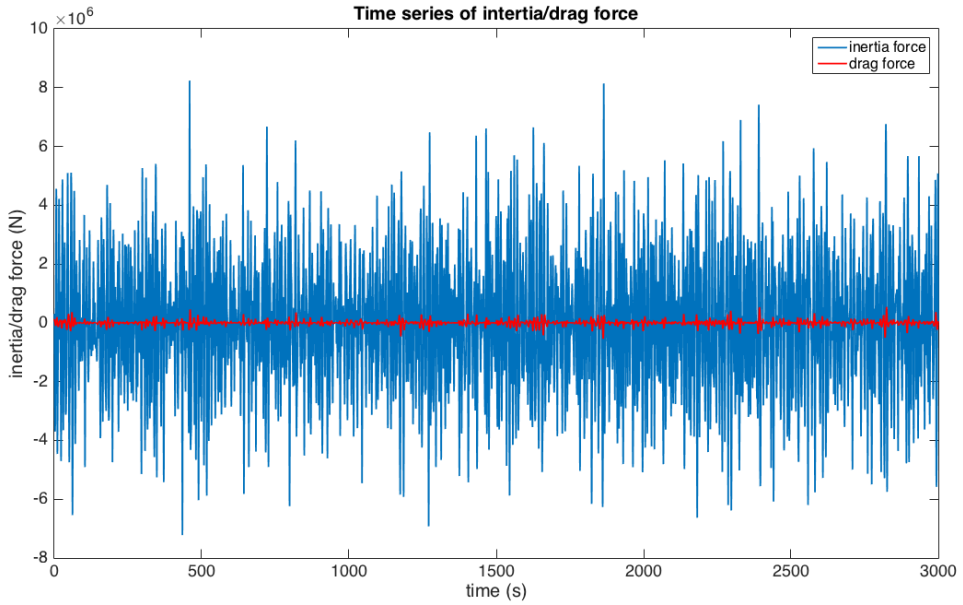

Figure 3.15 Inertia force and drag force loading from the Morison's equation

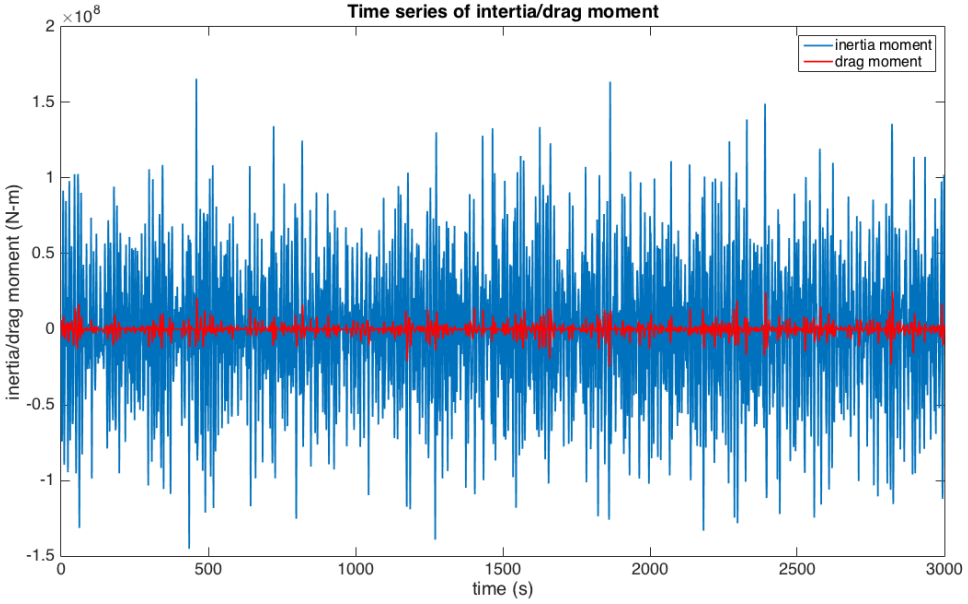

Figure 3.16 Inertia moment and drag moment loading from the Morison's equation

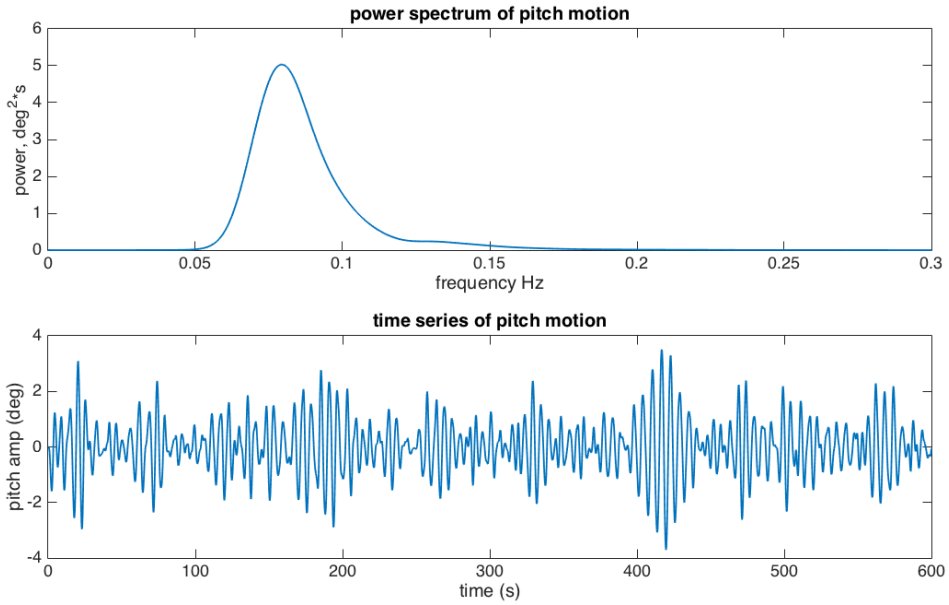

Figure 3.17 Predicted pitch motion by time-domain numerical model

From the results shown above, time-domain model also gives a relatively good prediction of motion in wave-frequency range. If raw data of input wave train can be provided, further analysis can go to the time-domain comparison. As a time-domain model, the solver of presented one highly sticks to the linear wave theory and the Morison's equation so that the simulation time is really fast compared with other commercial time-domain software. But it also brings about the lack of information for low-frequency range.

4. NONLINEAR NUMERICAL MODELS

Even though the two models given above show a good estimation of platform's hydrodynamic behaviors in frequency-domain range, the second-order response is unneglectable for detailed estimation. Because looking back to the measured surge and pitch motion spectra, energy distributed in low-frequency range is comparable with that of wave-frequency part. Moreover, after taking wind into consideration, the accurate estimation of low-frequency energy directly leads to a good estimation of whole floating wind turbine system under wind loading. Figure 4.1 and figure 4.2 shows the response of motions comparisons of selected experimental case with and without a steady wind, which proves the importance of second-order wave loading to spar-type floating turbine system. Here, it should be pointed out that, compared with data collected in MARIN (Figure 1.2), whose low-frequency surge motion was amplified while pitch motion was damped under wind loading, data collected in SKLOE showed a different tendency of wind influence on floating wind turbine system. In figure 4.1 and figure 4.2, both of surge and pitch motions were highly damped by wind effect. This is because in the former wave basin test, MARIN installed a motor for the turbine to allow control of the blade rpm in order to match the wind velocity and torque simultaneously in experiment scale; whereas for the later one, SKLOE only adjusted incoming wind velocity to match the designed torque without sticking to the designed wind velocity values.

Recalling the content in table 1.1, most of the OC3 participates start from the aerodynamic part in order to give a highly precise aerodynamic analysis of working wind turbine, together with only first-order hydrodynamic loadings. In this part of presented thesis, second-order wave loadings will be taken into consideration to perfectly simulate the floater response in whole frequency range. Later, wind effect of steady wind will be added.

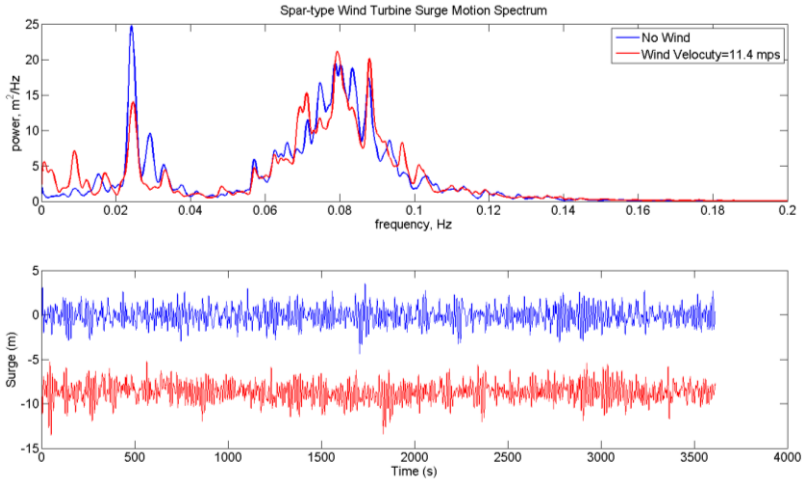

Figure 4.1 Surge motion under JONSWAP Spectrum Hs=7.1m, Tp=2.2s, gamma=2 with and without a 11.4 m/s steady wind

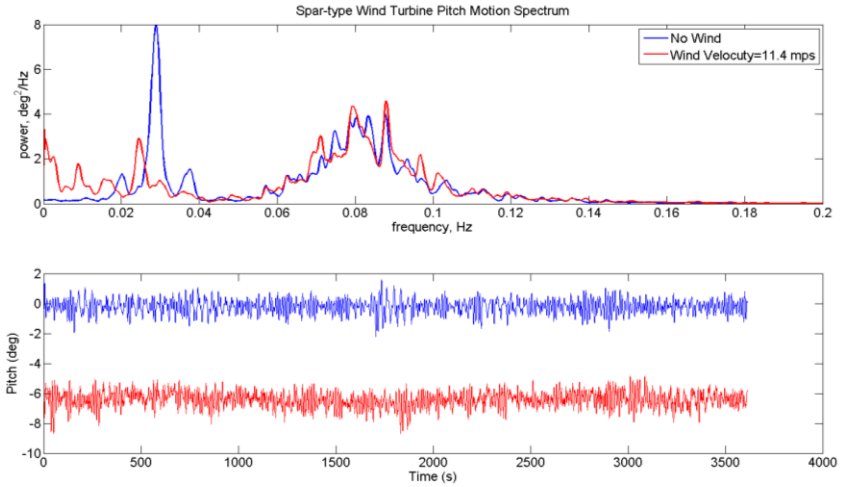

Figure 4.2 Pitch motion under JONSWAP Spectrum Hs=7.1m, Tp=2.2s, gamma=2 with and without a 11.4 m/s steady wind

WAMIT, a widely used hydrodynamic analysis tool, use panel theory based on potential wave theory. For second-order analysis, it can provide either mean-drift force by Newman's approximation based on first-order solution or full QTFs by starting from

fully nonlinear wave potential. In order to compare the difference between mean-drift QTFs and full QTFs for OC3-Hywind floater, WAMIT is used for second-order wave loading calculation for selected experimental cases.

Moreover, even though Agarwal and Jain (2003) developed a numerical model to estimate moored spar-type platform dynamic behavior under regular waves, a standard software in industry was selected for better time-domain simulation under irregular waves. Considering the mooring system, especially the delta line design, OrcaFlex is adopted as a mature commercial software to undergo the mooring system analysis. The coupled motion between Hywind spar-buoy and three mooring lines will be modeled. Figure 4.3 shows the floating wind turbine system built up in OrcaFlex, and figure 4.4 shows its mooring system. Thus, in this model, predicted mooring tension will also be compared with the measured one.

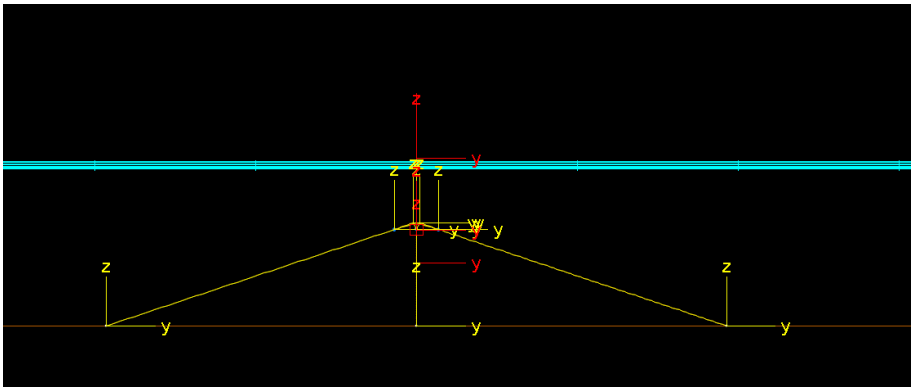

Figure 4.3 Floating wind turbine system built up in OrcaFlex

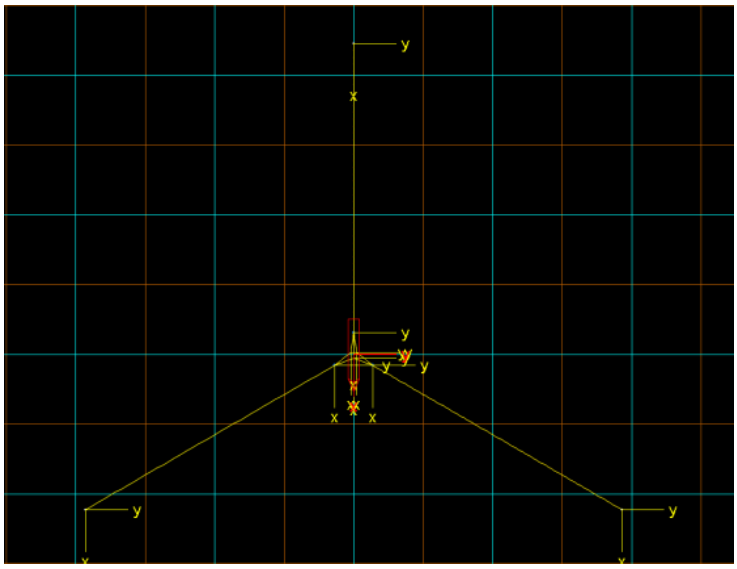

Figure 4.4 Mooring system of floating wind turbien system modeled in OrcaFlex

By inputing the hydrodynamic analysis results calculated from WAMIT into OrcaFlex, a whole simulation case will give all the response motions and tension of mooring in time series. Using the selected experiemtal case as an example, results with mean-drift QTFs and full QTFs are given in figure 4.5 and figure 4.6. For case using mean-drift QTFs, which only made use of the cross-multiplication terms of first-order wave theory, low-frequency motions of surge and pitch were well matched with experimental data. However, mooring tension force spextrum showed that low-frequency peak was underestimated. Whereas, for case using full QTFs, which was given by second-order WAMIT based on high-order wave theory, not only low-frequency surge and pitch motions, but mooring tension were all well matched. It should be noted that in the low-frequency range for mooring tension force spectrum, there's one more small peak induced by full QTFs which may reveal the overestimation of a certain motion.

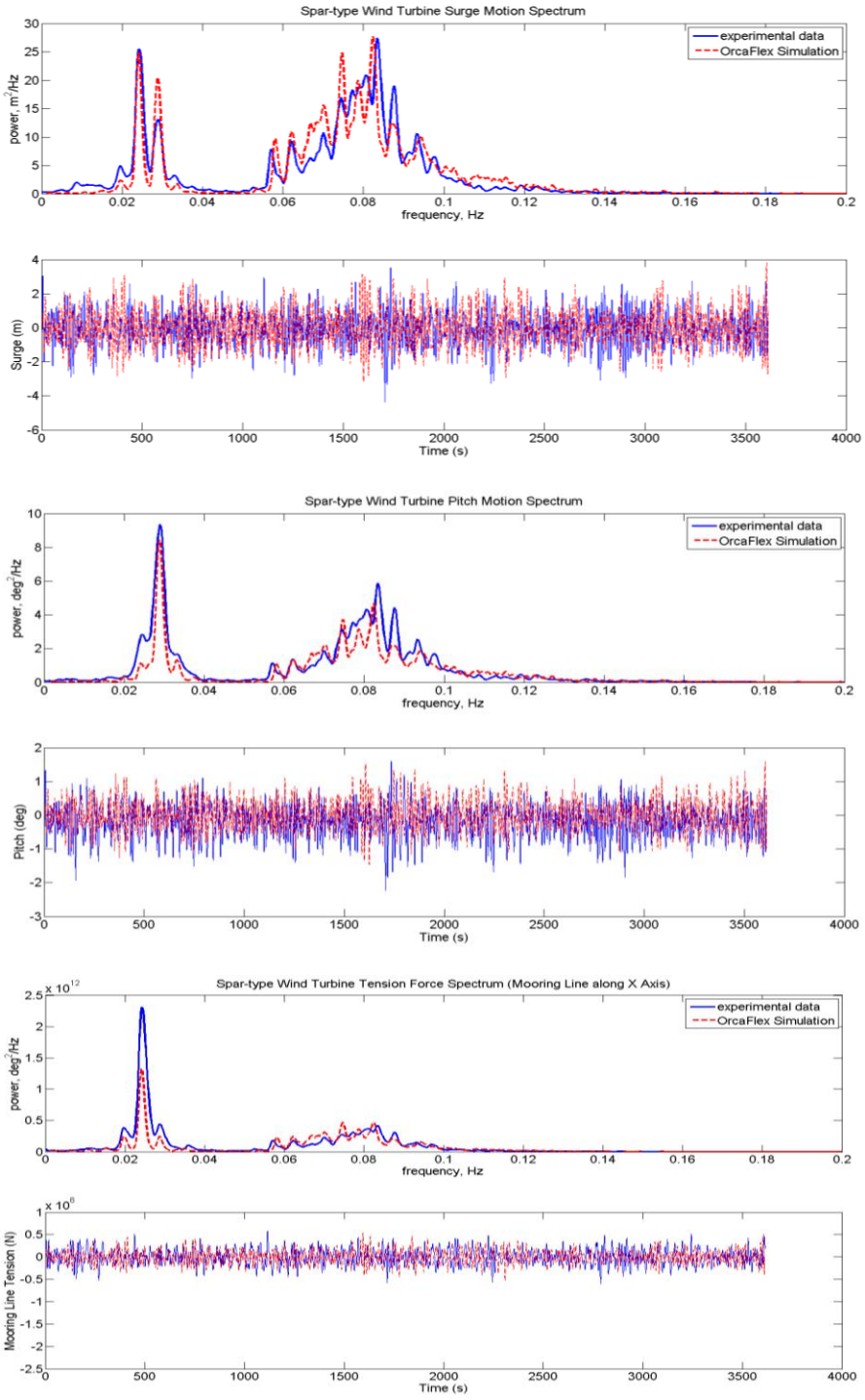

Figure 4.5 Surge and pitch motions and mooring line (along surge direction) tension calculated by mean-drift QTFs with JONSWAP Spectrum Hs=7.1m, Tp=2.2s, gamma=2

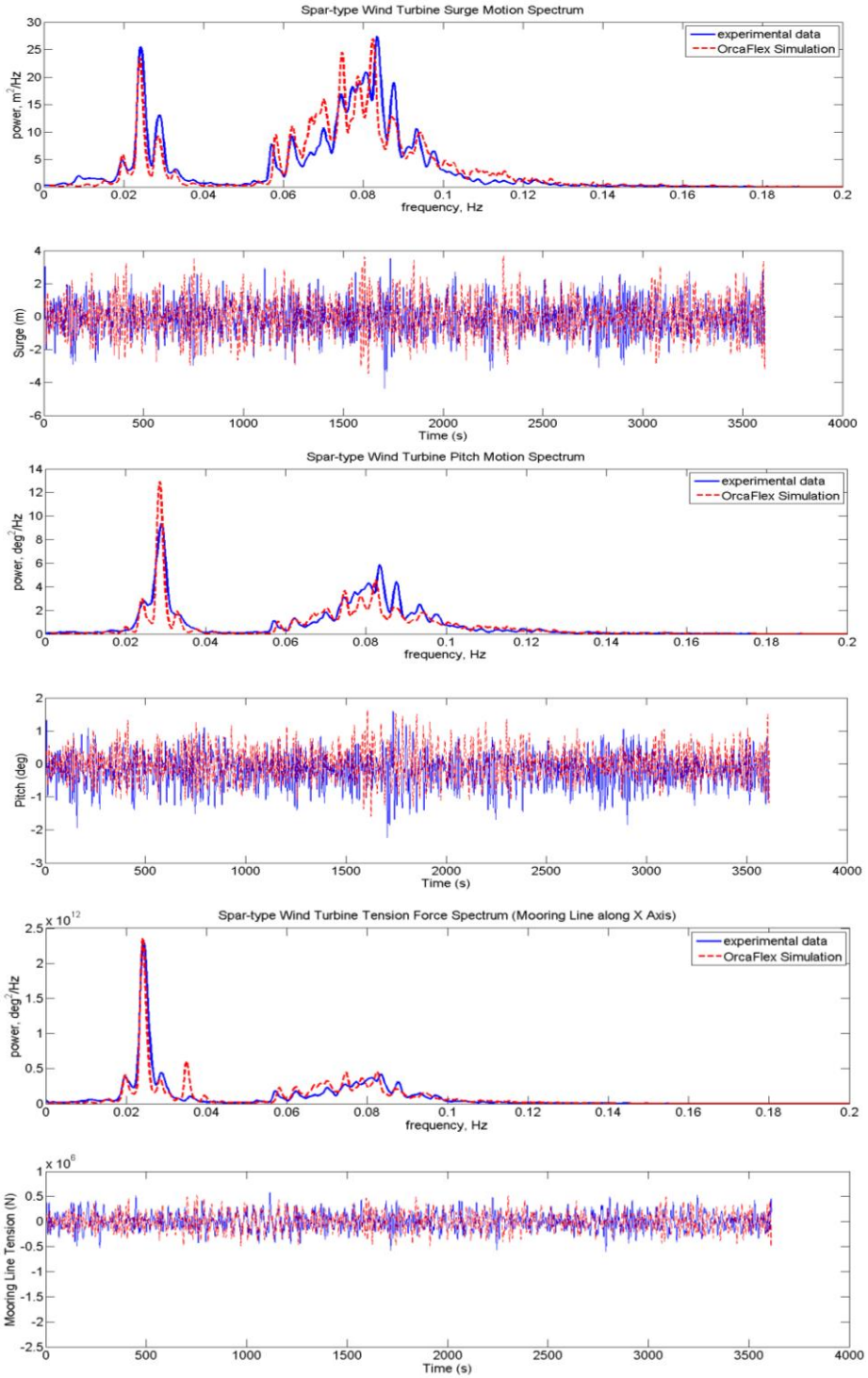

Figure 4.6 Surge and pitch motions and mooring line (along surge direction) tension calculated by full QTFs with JONSWAP Spectrum Hs=7.1m, Tp=2.2s, gamma=2

Based on this good estimation of hydrodynamic performance for whole frequency-range, the study can move on to the next step by introducing the steady wind. Even though there're lots of commercial software for aerodynamic analysis of wind turbine, most of them don't have a good communicating interface with these hydrodynamic software. Moreover, by running iteration for both aerodynamic and hydrodynamic software and exchange information between each other for each time step, simulation time will increase exponentially.

In this study, the module of wings in OrcaFlex is utilized for modulating the wind force. It should be noted that, even though steady wind was applied in the wave basin test, it is inevitable to have turbulence. So the wind velocity that pass through the wind turbine area is not absolute steady wind. By introducing the measured wind velocity time series, together with properly adjusted drag coefficient and lift coefficient for wings model, it shows a relatively good results in figure 4.7.

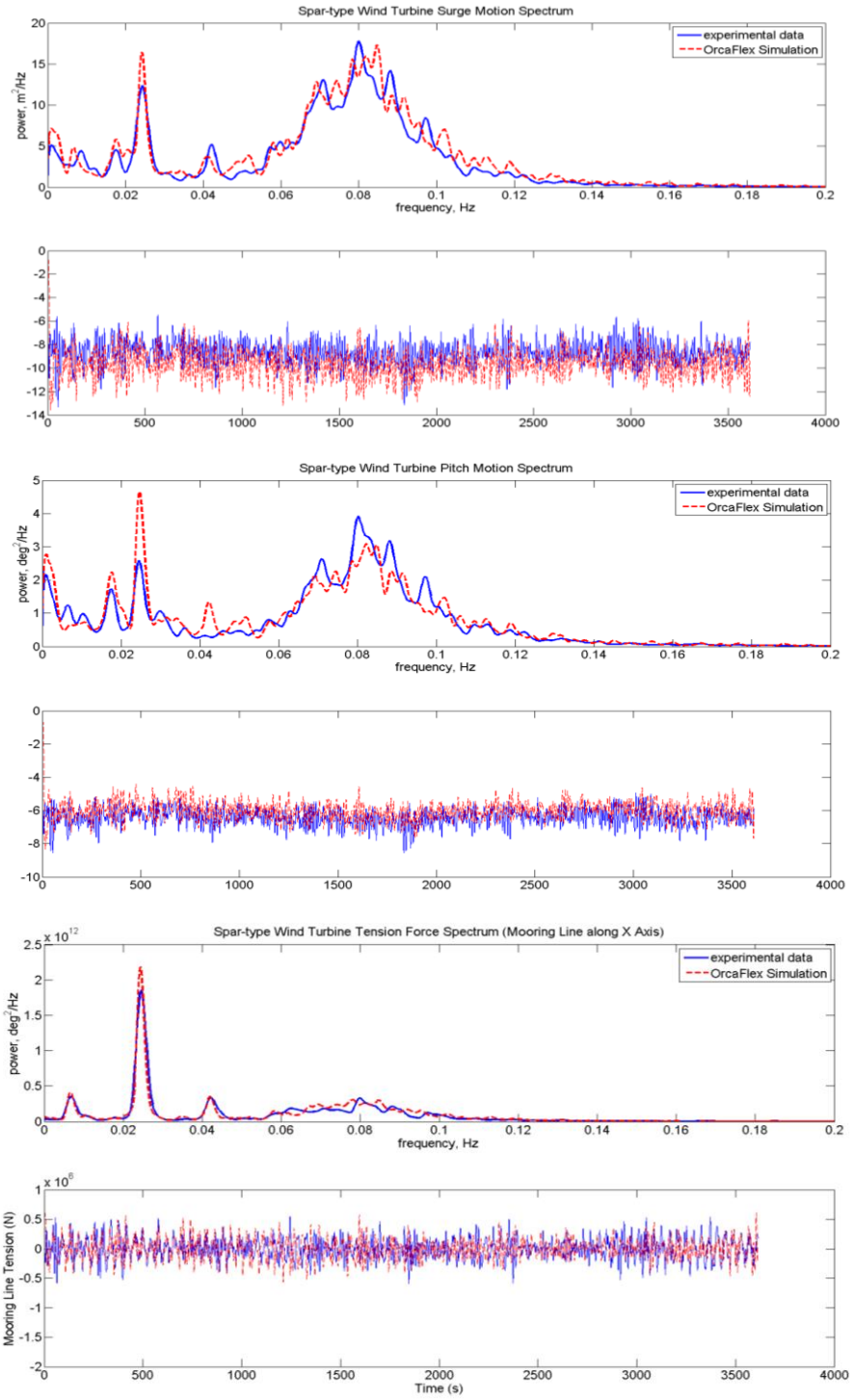

Figure 4.7 Surge and pitch motions and mooring line (along surge direction) tension calculated by full QTFs with JONSWAP Spectrum Hs=7.1m, Tp=2.2s, gamma=2 and 11.4 m/s steady wind

From the results predicted by the second-order model, it is proved that second-order hydrodynamic analysis plays an important role in the simulation of Hywind spar-type wind turbine floater. Both of the experiment and numerical results indicate a wind damping effect on low-frequency response while the wave-frequency response is almost not influenced. As to mooring tension, wind effect is mainly an offset of mean force, without too much influence on the force spectrum.

5. SUMMARY AND CONCLUSIONS

As a clean and renewable energy, wind technology has grown up fast into one of the main new energy types. However, land-based wind farm shows a great of shortages, including the occupation of limited land source, visual and acoustic impact on human activities, high cost for transmission due to its remote locations, et al. Thus, floating wind turbine in deep water areas is of great significance to largely increase the wind energy productivity. In recent years, coupled analysis for floating wind turbine makes it possible to simulate aerodynamic effect induced by working wind turbine atop a floating platform. However, the combination of nonlinear aerodynamic loading and high-order nonlinear wave loading limits the accuracy and efficiency of coupled analysis tools. This research study provides two types of numerical model to improve efficiency and accuracy.

The current research study first focused on developing a fast numerical tool which could estimate motion response in wave-frequency range based on the Morison's equation. It provided two options, including the one in frequency-domain that linearized the drag force term and the other one in time-domain that kept nonlinear drag force. This tool testified the effectiveness of the original form of Morison's equation to calculate the first-order hydrodynamic loadings. It should be pointed out that, for linearization of damping coefficient in frequency-domain and quick calculation of wave loading in time-domain, it neglected the relative motion between structure and fluid, thus the influence on fluid field by moving structure was missed. Thus, for the information out of wave-frequency range, second type of numerical tool should be applied.

The second type of numerical tool developed in this study involved high-order hydrodynamic loadings and detailed mooring line motion analysis by inducing standard industry software WAMIT and OrcaFlex. Thus, besides forced motion by wave force, it also predicted the motions in low-frequency range by mean-drift QTFs and full QTFs calculated by WAMIT. In addition, mooring lines were coupled with spar-floaters to be simulated simultaneously in time-domain, which gave a variety of mooring system

response predictions. Compared with the experimental data, the global motion response under hydrodynamic loading only was proved to be accurate in whole frequency range.

In addition, both wave basin tests conducted in MARIN and SKLOE for NREL 5MW baseline Hywind floating wind turbine showed a significant wind effect in low-frequency domain, whereas motion in wave-frequency domain remained almost unchanged. Thus, the second type of numerical tool was recommended for wind turbine analysis due to its good prediction of motion in whole frequency range. Since the vortex in wind field is inevitable, even experimental cases with steady wind velocity actually exerted a wind force varying with time. By introducing the wind velocity time series with measured wind drag coefficient, the second numerical tool further gave motions response under both wave and wind forces, which matched the experimental data quite well. Thus, the basis for revealing wind effect on a floating wind turbine system is a highly accurate hydrodynamic analysis with high-order formulations.

Overall, the new computation tools, which provided a preliminary analysis tool for quick spar-floater forced motion response in wave-frequency range and another accurate hydrodynamic analysis tool in whole frequency range for floating wind turbine study, proved to be accurate and efficient. The methodologies and studies presented in this thesis suggest that only with a good hydrodynamic analysis tool, wind effect and mooring line dynamic response could be well estimated.

REFERENCES

Agarwal, A. K. and Jain, A. K., 2003. Dynamic behavior of offshore spar platforms under regular sea waves. *Ocean engineering 30 (2003)*, 487-516.

Breton, S.P. and Moe, G., 2009. Status, plans and technologies for offshore wind turbines in Europe and North America. *Renewable Energy*, 34, 646-654.

Bulder, B. H., et al, 2002. Study to feasibility of and boundary conditions for floating offshore wind turbines. *Nov. 2002- CMC-R43, ECN, MARIN, Lagerway the Windmaster, TNO, TUD, MSC*.

Butterfield, S., Musial, W., Jonkman J., and Sclavounos, 2005. Engineering challenges for offshore wind turbines. *2005 Copenhagen Offshore Wind Conference, Copenhagen, Denmark, October 26-28, 2005*. NREL/CP-500-38776.

Duarte, T., Sarmento, A. JNA. And Jonkman, J.,2014. Effects of second-order hydrodynamic forces on floating offshore wind turbine. *AIAA SciTech 2014, National Harbor, Maryland, January 13-17, 2014.*

Duan, F., Hu, Z., and Niedzwecki, J. M., 2015. Model test investigation of a Spar floating wind turbine. *Marine Structures (submitted).*

Goupee, A. J., Koo, B., Kimball, R. W., Lambrakos K. F., and Dagher H. J., 2012. Experimental comparison of three floating wind turbine concepts. *Proceedings of the ASME 2012 31st International Conference on Ocean, Offshore and Arctic Engineering, Rio de Janeiro, Brazil, July 1-6, 2012*.

Jonkman, J. M. and Buhl, M. L., 2007. Loads analysis of a floating offshore wind turbine using fully coupled simulation. *Wind Power 2007 Conference & Exhibition, Los Angeles, California, June 3-6,* 2007.

Jonkman, J., Larsen, T. and et. al, 2010. Offshore code comparison collaboration within IEA wind task 23: phase IV results regarding floating wind turbine modeling. *European Wind Energy Conference (EWEC), Warsaw, Poland, April 20-23, 2010.*

Koo, B., Goupee, A. J., Lambrakos, K., and Kimball, R. W., 2012. Model test for a floating wind turbine on three different floaters. *Proceedings of the ASME 2012 31st International Conference on Ocean, Offshore and Arctic Engineering, Rio de Janeiro, Brazil, July 1-6, 2012*.

Karimirad, M. and Moan, T., 2012. Wave and wind-induced dynamic response of a spar-type offshore wind turbine. *Journal of Waterway, Port, Coastal, and Ocean Engineering*, Vol. 138, No. 1, 9-20.

Karimirad, M. and Moan T., 2011. Extreme dynamic structural response analysis of catenary moored spar wind turbine in harsh environmental conditions. *Journal of Offshore Mechanics and Arctic Engineering*, Vol. 133, 041103.

Karimirad, M., Meissonnier, Q., Gao, Z., and Moan, T., 2011. Hydroelastic code-to-code comparison for a tension leg spar-type floating wind turbine. *Marine Structure*, Vol. 24, 412-435.

Lee, K. H., 2005. Responses of floating wind turbines to wind and wave excitation. *M.S. Dissertation, Department of Ocean Engineering, Massachusetts Institute of Technology, Cambridge, MA, USA.*

Robert A. N., Jonkman, J. and et. al, 2013. Summary of conclusions and recommendations drawn from the DeepCWind scaled floating offshore wind system test campaign. *ASME 2013 32nd International Conference on Ocean, Offshore and Arctic Engineering, Nantes, France, June 9-14, 2013.*

Skaare, B., Hanson, T. D., Nielson, F. G., et al, 2007. Integrated dynamic analysis of floating offshore wind turbines. *European Wind Energy Conference and Exhibition*, Vol. 3, 1929-1939.

Smith, J. A. and Rieder, K. F., 1997. Wave induced motion of FLIP. *Ocean Engineering*, Vol. 24, No. 2, 95-110.

Utsunomiya, T. and Nishida, E., 2009. Wave response experiment on spar-type floating bodies for offshore wind turbine. *Proceedings of the 19th (2009) International*

Offshore and Polar Engineering Conference, Osaka, Japan, June 21-26, 2009, 378-383.

Utsunomiya, T., Matsukuma, H., Minoura, S., Ko, K., et al, 2013. At sea experiment of a Hybrid spar for floating offshore wind turbine using 1/10-scale model. *Journal of Offshore Mechanics and Arctic Engineering*, Vol. 135, 034503.

Utsunomiya, T., Sato, T., Matsukuma, H., and Yago, K., 2009. Experimental validation for motion of a spar-type floating offshore wind turbine using 1/22.5 scale model. *Proceedings of the ASME 2009 28th International Conference on Ocean, Offshore and Arctic Engineering, Honolulu, Hawaii, USA, May 31-June 5, 2009*.

Wayman E. N., Sclavounos, P. D., Butterfield, S., et al, 2006. Coupled dynamic modeling of floating wind turbine systems. *Offshore Technology Conference, Houston, Texas, May 1-4*, 2006.

Wang, C.M., Utsunomiya, T., Wee, S. C., and Choo, Y. S., 2010. Research on floating wind turbines: a literature survey. *Civil & Structural Engineering*, Vol. 3, No. 4, 267-277.

Wheeler, J. D., 1970. Method for calculating forces produced by irregular waves. *Journal of Petroleum Technology, Mar. 1970*, 359-367.

Xing, Y., Karimirad, M. and Moan T., 2014. Modeling and analysis of floating spar-type wind turbine drivetrain. *Wind energy*, Vol. 17, 565-587.

APPENDIX

CODING OF LINEAR MODELS IN MATLAB

1. Linearized Numerical Model in Frequency-domain

```
% FLIP Method to Calculate LC4 (White Noise Wave)
% He Yang
% 2014/12

clear all;

% FLIP Frequency Domain Calculation
% He Yang
% 2014/12

clear all;

% Parameters of FLIP
   dz=0.5; % unit:m
   z=-120:dz:0;
   Ci=1; % Added mass coeff.
   Cd=0.8; % Drag coeff.
   ro=1025; %Kg/m3;
```

```
g=9.81; % m/s2

M=8066110; %Kg
M_Dis=ro*(pi*3.25^2*4+pi*4.7^2*108+8*pi/3*(3.25^2+4.7^2+3.25*4.7)); % water
    displacement
Mi=M+Ci*M_Dis; %total mass including spar and added mass
I_pitch=23161872557; % total pitch inertia with respect to spar center of mass
gamma_f=sqrt(I_pitch/M); % radius of gyration: m

zf=-78.947; %m

% Create intersection radius and area
r1=3.25*z(z>-4).^0;
r2=3.25-(z(z>-12&z<=-4)+4)*29/160;
r3=4.7*z(z<=-12).^0;
r=[r1 r2 r3];
r=sort(r,'descend');
A=pi*(r.*r);
A0=pi*3.25^2; % waterline area

% calculate buoyancy center
zbb=ro/M_Dis*trapz(z,z.*A);
```

```
    gamma_bb=sqrt(trapz(z,(z-zbb).^2.*A)*ro/M_Dis);


    zcc=(M*zf+M_Dis*Ci*zbb)/Mi;
    gamma_cc=sqrt((I_pitch+M*(zf-zcc).^2+(gamma_bb.^2+(zbb-zcc).^2)*M_Dis)/Mi);


% Load time series of wave elevation
    data_LC4=xlsread('JONSWAP_WAVE_7.1m_12.1s.xlsx');
    time=data_LC4(:,1);
    eta_0=data_LC4(:,26);



% FFT of wave elevation
    [DeltaF, ff, fft_eta, amp_eta, pow_eta]=create_spectrum(time,eta_0);
    w=2*pi*ff;
    k=w.^2/g;


    figure(1)
    plot(w/2/pi,pow_eta)
    xlim([0 0.3])
    title('LC4 wave spectrum')
    xlabel('frequency (Hz)')
    ylabel('Amplitude (m^2*s)')
```

```
% Calculate forces and moments

% (1) Calculate forces
FC_bar=abs(-70-zcc);
GB_bar=abs(zbb-zf);
K=10^6/(5.2-2.75); % horizontal stiffness of mooring system

for i=1:length(z)
   V_z(i)=sqrt(trapz(w,amp_eta.^2.*w.^2.*exp(2*w.^2/g*z(i))));
end
Dv_z=Cd*V_z;

for i=1:length(w)
Fw_1(i)=ro*g*(1+Ci)*trapz(z,A.*exp(k(i)*z));
Fw_2(i)=ro*g*sqrt(-1)*2*pi/w(i)*trapz(z,exp(k(i)*z).*Dv_z.*r);
Fw(i)=Fw_1(i)+Fw_2(i);
end

CC1=2*pi*ro*trapz(z,Dv_z.*r);
CC2=2*pi*ro*trapz(z,(z-zcc).*Dv_z.*r);
```

```
% (2) Calculate moments
for i=1:length(w)
Tw_1(i)=ro*g*(1+Ci)*trapz(z,(z-zcc).*A.*exp(k(i)*z));
Tw_2(i)=ro*g*sqrt(-1)*2*pi/w(i)*trapz(z,(z-zcc).*exp(k(i)*z).*Dv_z.*r);
Tw(i)=Tw_1(i)+Tw_2(i);
end

DD1=2*pi*ro*trapz(z,(z-zcc).*Dv_z.*r);
DD2=2*pi*ro*trapz(z,(z-zcc).^2.*Dv_z.*r);

Ksh=pi/64*ro*g*3.25^4+M*g*GB_bar;
K_theta=K*FC_bar^2-(M_Dis-M)*g*FC_bar-Ksh;

eta_x=sqrt(-1)*k.*fft_eta;

for i=1:length(w)
coef1(i)=K-Mi*w(i)^2-sqrt(-1)*w(i)*CC1;
coef2(i)=-sqrt(-1)*w(i)*CC2-K*FC_bar;
coef3(i)=-eta_x(i)*Fw(i);

coef4(i)=K*FC_bar-sqrt(-1)*w(i)*DD1;
coef5(i)=-K_theta-Mi*gamma_cc^2*w(i)^2-sqrt(-1)*w(i)*DD2;
```

```
coef6(i)=-eta_x(i)*Tw(i);

x_w(i)=(coef3(i)*coef5(i)-coef2(i)*coef6(i))/(coef1(i)*coef5(i)-coef2(i)*coef4(i));
theta_w(i)=(coef1(i)*coef6(i)-coef3(i)*coef4(i))/(coef1(i)*coef5(i)-coef2(i)*coef4(i));
end
x_w(1)=0;
theta_w(1)=0;
x_w_amp=abs(x_w);
theta_w_amp=abs(theta_w);

x_w_amp=x_w_amp';
theta_w_amp=theta_w_amp';

figure(2)
% smoothing surge amp
for k=1:8
for i=3:length(x_w_amp)-2;
x_w_amp(i,:)=1/5*(x_w_amp(i-2,:)+x_w_amp(i-
    1,:)+x_w_amp(i,:)+x_w_amp(i+1,:)+x_w_amp(i+2,:));
end
end
% smoothing pitch amp
```

```
for k=1:8
for i=3:length(theta_w_amp)-2;
theta_w_amp(i,:)=1/5*(theta_w_amp(i-2,:)+theta_w_amp(i-
    1,:)+theta_w_amp(i,:)+theta_w_amp(i+1,:)+theta_w_amp(i+2,:));
end
end

subplot(1,2,1)
plot(w/2/pi,x_w_amp)
xlim([0 0.3])
title('Surge Motion of Body-coordinate Origin')
xlabel('frequency Hz')
ylabel('surge amp (m)')
hold on
subplot(1,2,2)
plot(w/2/pi,theta_w_amp*360/2/pi)
xlim([0 0.3])
title('Pitch Motion of Body-coordinate Origin')
xlabel('frequency Hz')
ylabel('pitch amp (deg)')

zr=zcc-x_w_amp./theta_w_amp;
```

```
figure(3)
plot(w,zr)
title('Rotation center varying with frequency')
xlabel('frequency (rad/s)')
ylabel('ratation center (m)')
xlim([0.25 2])



figure(4)
xxx_w=x_w+abs(zcc)*theta_w;
xxx_w_amp=abs(xxx_w);
pow_xxx_w=0.5*xxx_w_amp.*xxx_w_amp./DeltaF;
pow_xxx_w=pow_xxx_w';



% input raw data and select interested one
datairregular=load('no_wind,no_current,Hs=7.1m,Tp=12.1s-Full.dat');
datairregular(:,23:25)=1000*datairregular(:,23:25);
Col_Num=[2 4 6 8 9 10 23 24 25 26];

% Time resolution of time series
Taxis=datairregular(:,1);
```

```
    L=length(Taxis);
    DeltaT=Taxis(L,1)/(L-1);

% Filter the data in butterworth filter
    i_filt=1;
    if i_filt==1, butterworth_filter; end

% calculate the power spectrum
    for i=1:10;
    data(:,i)=datairregular(:,Col_Num(i))-mean(datairregular(:,Col_Num(i))); %remove
          the offset

% apply hanning window
    hanning_win=hanning(floor(L/8));
    n_han = length(hanning_win);
    pos=1;

    while (pos+n_han <= L)

       data_win(pos:pos+n_han-1,i)= data(pos:pos+n_han-1,i).*hanning_win;
       pos = pos + n_han/2;
```

```
    end

    [f, pow_data(:,i)]=power_spectrum(L,DeltaT,data_win(:,i));
    end

% smoothing
    for k=1:15
    for i=3:length(pow_data)-2;
    pow_data(i,:)=1/5*(pow_data(i-2,:)+pow_data(i-
        1,:)+pow_data(i,:)+pow_data(i+1,:)+pow_data(i+2,:));
    end
    end

% smoothing surge spectrum
    for k=1:3
    for i=3:length(pow_xxx_w)-2;
    pow_xxx_w(i,:)=1/5*(pow_xxx_w(i-2,:)+pow_xxx_w(i-
        1,:)+pow_xxx_w(i,:)+pow_xxx_w(i+1,:)+pow_xxx_w(i+2,:));
    end
    end

    figure(5)
```

```
plot(f,pow_data(:,1),'LineWidth',1.2)
hold on
plot(w/2/pi,pow_xxx_w,'r--')

xlim([0 0.3])
xlabel('frequency Hz')
ylabel('power, m^2*s')
title('Prediction of Surge Motion in SWL by Numerical Model in Frequency-domain')
legend('Experimental Data', 'Numerical Model in Frequency-domain')
```